Chemical Thermodynamics and Thermal Analysis 23 (2026) 100349

Contents lists available at ScienceDirect

Chemical Thermodynamics and Thermal Analysis

journal homepage: www.elsevier.com/locate/ctta

Structure-Property Insights into Piperazine-Based Protic Ionic Liquids: Role of Carboxylate Anion Chain Length

K. Devaiah [1,a], Neha Rani Kumar [1,b,*], Ramesh L. Gardas [a,c,*]

[a] Department of Chemistry, Indian Institute of Technology Madras, Chennai-600036, India
[b] Department of Chemistry, Dhemaji College, Dhemaji, Assam-787057, India
[c] School of Sustainability, Indian Institute of Technology Madras, Chennai 600036, India

ARTICLE INFO

Keywords:
Ethyl piperazine
Protic Ionic Liquids (PILs)
Physicochemical Properties
DFT

ABSTRACT

Piperazinium cation-based protic ionic liquids (PILs) have important applications in diverse fields like catalysis, coal desulfurization, SO_2 capture, microemulsion formation, and solid electrolytes for batteries. Despite the broad applications, their practical applications are hindered by the lack of detailed insights into the factors that influence the molecular associations and the macroscopic properties. Here we report the synthesis of a series of piperazine-based PILs, viz. [EtPIPZ][For], [EtPIPZ][Ace], [EtPIPZ][Prop], [EtPIPZ][But], [EtPIPZ][Pent], and [EtPIPZ][Hex] by varying the carboxylate anion chain length. The PILs were synthesized by the direct neutralization strategy and were characterized by NMR, ATR-FTIR, and mass spectroscopic techniques. The key physicochemical properties, such as density *(ρ)*, speed of sound *(u)*, viscosity *(η)*, refractive index *(n_D)*, and ionic conductivity *(σ)*, were measured in the temperature range of 293.15 K to 323.15 K and pressure 0.1 MPa for the room temperature PILs [EtPIPZ][For], [EtPIPZ][Prop], [EtPIPZ][But], and [EtPIPZ][Pent]. The other associated thermodynamic parameters were derived to get insights into the ion-ion interactions and free volume *(L_f)* characteristics. It was found that an increase in the alkyl chain length of the carboxylate anion leads to reduced density, refractive index, and ionic conductivity and an increase in viscosity, molecular volume *(V)*, isentropic compressibility *(β_s)*, and free volume *(L_f)*. These trends indicate diminished packing efficiency and enhanced ion mobility constraints in PILs with longer alkyl chains. In addition, Density Functional Theory (DFT) calculations including HOMO-LUMO energy levels, electrostatic potential (ESP) surfaces, interaction energies, and reduced density gradient (RDG) analysis, revealed progressively weaker non covalent cation-anion interactions with increasing alkyl chain length. The combined experimental and computational results establish a comprehensive structure-property relationship established here will help tailor the properties of piperazine-based PILs for electrochemical, separation, and solvent-based applications.

1. Introduction

Since their first discovery in 1914 by Paul Walden, ionic liquids (ILs) have emerged as a versatile class of materials owing to their peculiar properties, such as negligible vapour pressure, wide electrochemical windows, and tunable physicochemical properties[1,2]. The physicochemical properties of ILs can be tuned by modifying the structure of cations and anions, such as by varying the length of the alkyl chain either on the cation or anion, which disrupts packing and alters the hydrogen bonding[3–5]. Advanced functionalization strategies for fine-tuning the properties of ILs include the introduction of specific functional groups such as hydroxyl (-OH), ether (-O-), or amino (NH_2-) moieties on either cations or anions to reduce viscosity and enhance conductivity[6–9]. The rational modification of IL structures has led to their application in diverse arenas such as gas separation, electrochemical energy storage, catalysis, advanced solvent systems, etc [10–15]. Amongst the different classes of ILs, protic ionic liquids (PILs)-formed by the acid-base neutralization reaction between Bronsted acids and Bronsted bases have garnered wide attention due to their structural simplicity, strong hydrogen-bonding networks, and potential for enhanced proton and ion transport[16]. Despite the advances in the field, establishing structure-property relationships in PILs has been an

* Corresponding authors.
E-mail addresses: nehakumar0926@gmail.com (N.R. Kumar), gardas@iitm.ac.in (R.L. Gardas).
[1] These authors contributed equally to the work.

https://doi.org/10.1016/j.ctta.2026.100349
Received 26 May 2026; Received in revised form 14 July 2026; Accepted 19 July 2026
Available online 20 July 2026

arduous task. In contrast to aprotic ILs, where Coulombic interactions are the dominant forces, PILs exhibit a complex blend of electrostatic interactions, hydrogen bonding, and dispersion forces[17–19]. These competing interactions significantly influence the properties such as conductivity, viscosity, thermal stability, etc., in ILs. Consequently, systematic insights that isolate the influence of individual structural parameters are necessary for the rational design of PILs for application-specific requirements.

Piperazinium cation-containing ILs offer a structurally distinct platform for the design of PILs due to the presence of two nitrogen atoms [20]. This introduces the possibility of multiple hydrogen-bond donor and acceptor sites, thereby strengthening the interactions between cation and anion and alter the ion association behaviour. In recent years, piperazinium-based ILs have found applications in desulfurization of coal, SO_2 capture, catalysis in organic synthesis, electrolytes etc[21–25]. Despite the promising possibilities, piperazinium-based PILs remain unexplored, and existing reports largely focus on synthesis or isolated properties. Detailed insights into the influence of molecular structure on the physicochemical properties and transport behaviour for piperazinium-based ILs are a potential area to explore. Carboxylate anions provide an ideal framework to modulate the properties of ILs such as viscosity, melting point, conductivity, H-bonding, basicity etc, making them potential candidates for applications in catalysis, extraction, and gas capture[26–29]. The carboxylate anion chain length can be systematically varied, keeping the ionic head group unchanged, and the influence on the structure-property relationships can be explored. In fact, these studies have been performed on certain imidazolium, ammonium, and phosphonium-based PILs[30–32]. Analogous experimental studies on piperazinium-based ILs are missing, and a unified experimental and theoretical assessment of how anion chain length governs ion mobility, packing efficiency, free volume, and energetic barriers is the need of the hour.

The present study addresses this gap by reporting a systematic investigation of a homologous series of N-ethylpiperazinium alkanoate PILs, in which the carboxylate anion chain length is varied from one carbon to six carbons. The synthesis of the PILs was accomplished by an acid-base neutralization reaction between N-ethyl piperazine and the corresponding carboxylic acid. The physicochemical and transport properties, including density (ρ), speed of sound (u), viscosity (η), refractive index (n_D), and ionic conductivity (σ) were measured over wide temperature ranges. The obtained experimental data were further used to compute other thermodynamic parameters related to ion–ion interactions, molecular packing, and free volume (L_f) etc. Besides the experimental work, Density Functional Theory (DFT) calculations including optimised molecular geometries, HOMO-LUMO energy levels, electrostatic potential (ESP) surfaces, interaction energies, and reduced density gradient (RDG) analysis were performed to gain molecular level insights into the electronic structure and non-covalent cation-anion interactions. The systematic experimental and theoretical investigations presented herein are aimed at establishing structure-property relationships and identifying the molecular interactions responsible for the thermodynamic and transport behaviour of piperazinium-based PILs. This study is also expected to provide valuable insights into the possible applications of synthesized PILs in gas capture, electrolyte formulations, catalysis, desulfurization of fuels, etc.

2. Experimental section

2.1. Materials

1-ethylpiperazine was acquired from Spectrochem, India. Formic acid, acetic acid, propanoic acid, and hexanoic acid were purchased from SRL, whereas butanoic acid and pentanoic acid were purchased from Loba Chemie and Avra, respectively. All of the chemicals used in the synthesis were of the highest purity (≥98%) and analytical grade and were used as such without any further purification. The purity (mass percentage), source and CAS Number of the chemicals are given in Table 1.

2.2. Synthesis of ionic liquids

N-ethyl piperazinium alkanoates were synthesized by direct neutralization of N-ethyl piperazine (1 equivalent) with the alkanoic acid (1.1 equivalent) as shown in Figure 1. The mixture of N-ethyl piperazine (10g, 1 equivalent) with ethanol (50 mL) was loaded into a 100 mL three-necked round-bottomed flask in an ice-water bath. A solution of alkanoic acid (1.1 equivalents) in ethanol (15 mL) was added dropwise into the flask, and the mixture was stirred for 30 min. The ice bath was removed, and the reaction mixture was stirred at room temperature for 5 hours. The entire reaction was performed under inert conditions. After the reaction was complete, ethanol was removed under pressure using a rotary evaporator. The obtained product was dried under vacuum at 338.15 K for 5 hours. All the products [EtPIPZ][For], [EtPIPZ][Ace], [EtPIPZ][Prop], [EtPIPZ][But], [EtPIPZ][Pent], [EtPIPZ][Hex] were obtained in more than 90% yields (Figure S1 and Figure S2).

The acetate and hexanoate-based ILs were obtained as solids at room temperature, whereas the formate, propanoate, butanoate, and pentanoate ILs were room temperature ionic liquids (RTILs). The images of the synthesized ILs are shown in Figure 2, and their IUPAC name, abbreviation used, molecular weight, physical state, solubility and the purity of synthesized PILs were determined by 1H NMR and the residual water content of the PILs was measured by Karl Fischer (KF) titration and decreased with increasing alkyl chain length from 2753-2259 ppm with an increase in the length of alkyl chain. The calculated purity values using 1H NMR and KF titration have been listed in Table 2.

2.3. Characterisation of ILs

The synthesised EtPIPZ-based ILs were characterised by Nuclear Magnetic Resonance (NMR), High Resolution Mass Spectrum (HRMS), and Attenuated Total Internal Reflectance-Fourier Transform Infra-red (ATR-FTIR) techniques. For the synthesised ILs, the NMR spectra were measured on a Bruker Avance 500 MHz NMR spectrometer by using deuterated chloroform ($CDCl_3$), and tetramethyl silane (TMS) was used as the internal reference. In ^{1}H NMR, the $CDCl_3$ peaks are observed at δ values 7.26 ppm and 77.06 ppm for ^{1}H and ^{13}C NMR, respectively. The HRMS was obtained using an Agilent 6545 Q-TOF LC/GC instrument. The samples were prepared by diluting 0.5 ml of the ILs in a 2 ml methanol solution before injection into the instrument. The ion source operated in dual mode, utilizing both AJS ESI in both positive and negative modes. The instrument's operating conditions include a gas temperature of 498.15 K a drying gas flow rate of 5 L per minute, a nebulizer pressure of 35 psi, a sheath gas temperature of 498.15 K and a sheath gas flow rate of 8 L per minute. The ATR-FTIR spectra were recorded using a Bruker Tensor II FTIR spectrophotometer. The FTIR spectrum was first calibrated using air or standard samples from BRUKER, UK, along with a blank spectrum.

Table 1
List of chemicals used for the ILs sysnthesis.

Name	Purity (mass percentage)[a]	Source	CAS Number
1-ethylpiperazine	99%	Spectrochem	5308-25-8
Formic acid	98%	SRL	64-18-6
Acetic acid	99.5%	SRL	64-19-7
Propanoic acid	99.5%	SRL	79-09-4
Butanoic acid	99%	Loba Chemie	107-92-6
Pentanoic acid	98%	Avra	109-52-4
Hexanoic acid	99%	SRL	142-62-1

[a] as declared by the supplier and used as received

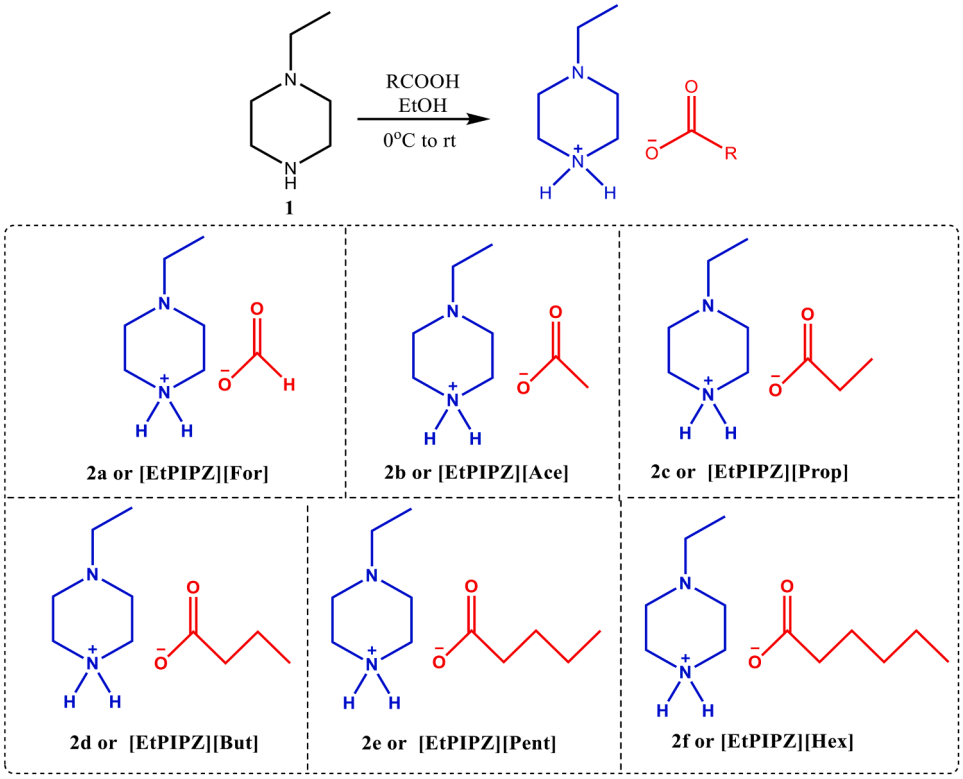

Figure 1. Synthesis of piperazinium-based ILs containing carboxylate anions of varying chain length.

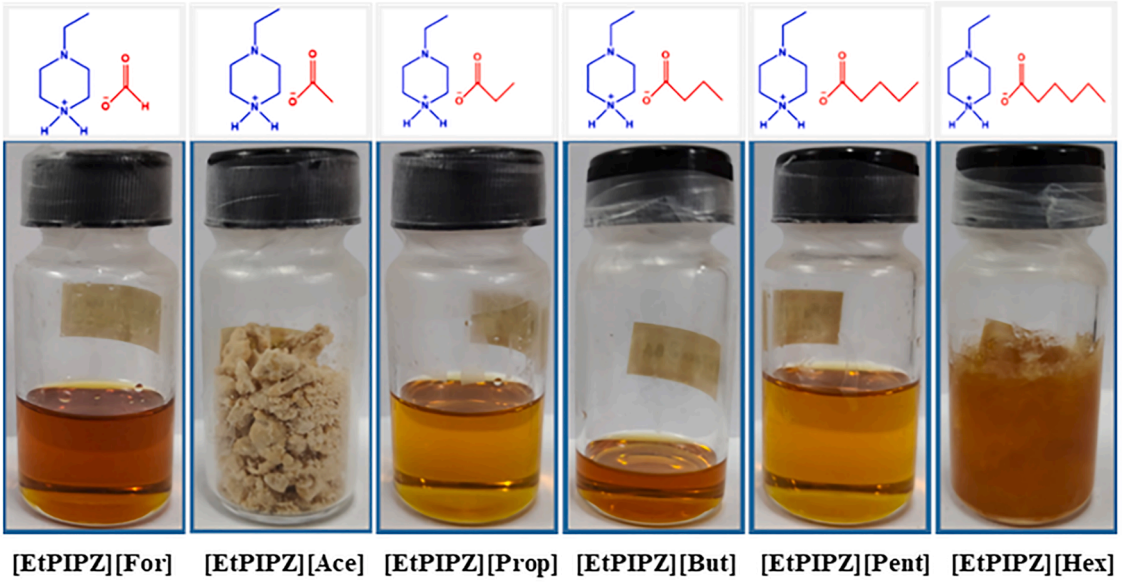

Figure 2. Images of the EtPIPZ-based ILs.

2.4. Density, speed of sound, and viscosity

The density and speed of sound of the synthesized ILs were analysed by employing Anton Paar (DSA 5000M) digital density and sound velocity meter. The instrument has the speciality of measuring both parameters simultaneously. It consists of a polymer cell that operates and controls the propagation time. The instrument can measure the speed of sound of a liquid within the range 1000-2000 $m.s^{-1}$, and the temperature and pressure range are 273.15 K-343.15 K and 0-3 bar, respectively. It maintains precise temperature control using the PT-100 sensor with a precision of 0.01 K. The instrument needs to be calibrated before use, and the calibration is accomplished by using Millipore water and drying the instrument with air at near room temperature. The analysis requires 3-4 mL of each sample, and it is carefully injected through the measurement cell using a syringe ensuring the absence of air bubbles. The viscosity of the synthesised EtPIPZ-based ILs was measured by using an Anton Paar Lovis 2000ME viscometer at temperature ranges from 293.15 to 323.15 K with an interval of 5 K. The viscometer was calibrated with standard oils supplied by Anton Paar Co., Austria. The capillary tube is first filled with a ceramic ball, followed by the IL. It is to

Table 2
IUPAC name, abbreviations and purity of the piperazinium-based PILs.

Abbreviation	Molecular weight	Physical State	Solubility	Purity (Mass fraction) [a]	Water Content (ppm) [b]
[EtPIPZ][For]	160.21	Viscous liquid	MeOH, EtOH, H_2O	≥ 0.97	2753
[EtPIPZ][Ace]	174.13	Amorphous solid	MeOH, EtOH, H_2O	≥ 0.99	2557
[EtPIPZ][Prop]	188.15	Viscous liquid	MeOH, EtOH, H_2O	≥ 0.99	2476
[EtPIPZ][But]	202.29	Viscous liquid	MeOH, EtOH, H_2O	≥ 0.99	2490
[EtPIPZ][Pent]	216.32	Viscous liquid	MeOH, EtOH, H_2O	≥ 0.99	2391
[EtPIPZ][Hex]	230.34	Crystalline solid	MeOH, EtOH, H_2O	≥ 0.99	2259

[a] calculated by using ^{1}H NMR
[b] Water content calculated using KF titration with standard uncertainty ±30 ppm

be ensured that air bubbles are absent when filling, and the viscosity is measured based on the movement of the ceramic ball and the average time taken to travel from one end to another in the capillary during the analysis. The relative error of the analysis is approximately 1%.

2.5. Thermogravimetric analysis and differential scanning calorimetry

Thermogravimetric Analysis (TGA) was conducted on an Erhard Mettler TGA instrument. It continuously measures the mass of a synthesised EtPIPZ-based ILs over a temperature range from 298 K to 600 K. From the measured Data, one can analyse the thermal breakdown of synthesised ILs. The desired quantity (50 mg) of EtPIPZ-based ILs was heated on a platinum-coated pan under an inert atmosphere (20 mL/min flow rate) at atmospheric pressure from 298 K to 600 K at a heating ramp rate of 10 K/min. Differential Scanning Calorimetry (DSC) was performed by using a differential scanning calorimeter (TA Instruments, DSC Q200). High-purity zinc (transition temperature of 692.15 K) supplied by TA Instruments was used as a reference material to calibrate the instrument. The samples were contained in sealed crucibles, with a heating rate and cooling rate of 10°C/min.

2.6. Refractive index

Refractive index (n_D) is defined as the ratio of the speed of light in vacuum to the speed of light in an optical medium. The refractive index of the synthesised EtPIPZ-based ILs was measured using a Refracto-30GS refractometer over the temperature range 293.15 to 323.15 K at 5 K intervals. Temperature control was maintained using a high-precision temperature refrigerated circulator (JULABO F200). The Refractometer was calibrated with Millipore water before and after each set of measurements. The standard uncertainty of refractive index was 0.001, and the temperature uncertainty was $u(T) = 0.01$ K

2.7. Ionic conductivity

Ionic conductivity (σ), arises from the movement of charged ions under an applied electric field. It is an important parameter used for getting insights into the transport properties as well as the electrochemical properties of ILs. The ionic conductivity for the synthesized ETPIPZ-based ILs was measured by using a Systronics Conductivity Meter 304 over the temperature range of 293.15 - 323.15 K at an atmospheric pressure of 0.1 MPa. The temperature of the system was controlled by using a high-precision refrigerated circulator (JULABO 200F), and the conductivity meter was calibrated by using a standard 0.1 M KCl solution.

2.8. Theoretical studies

The Density Functional Theory (DFT) calculations were performed using the Gaussian 16 software package. The synthesised EtPIPZ-based ILs were optimised at the 6-311 ++ G (d, p) level of theory. DFT analysis of the ILs is expected to provide detailed information about molecular-level interactions, including structural, energetic, and electronic properties. Structural properties provide information about the optimised geometry corresponding to the minimum energy of the cation-anion pair. Geometry optimization also helps in analysing and confirming the most stable conformation of the system, and enables the analysis of intermolecular interactions such as hydrogen bonding between the cation-anion pair. The energetic properties give insights into the stability and the strength of ion pairing. These include the interaction energy and binding energy that quantifies the strength of attraction between the cation and the anion. Energetic parameters also provide information about the thermodynamic stability and may correlate with solvation behaviour and thermal stability. Electronic properties involve the analysis of charge transfer and frontier molecular orbitals. The energies of the highest occupied molecular orbital (HOMO) and lowest unoccupied molecular orbital (LUMO) give an idea about the chemical reactivity, electron-donating and electron-accepting abilities, and the overall electronic stability. Finally, the electrostatic surface potential (ESP) maps the electron-deficient (positive) and electron-rich (negative) regions of the molecule, thereby identifying potential reactive sites and regions involved in intermolecular interactions.

3. Results and discussion

It is noteworthy that, unlike many previously reported homologous protic ionic liquid series in which a continuous liquid-state trend is observed from lower chains to higher chains,[33,34] the present N-ethylpiperazinium carboxylate family exhibits an unusual behaviour. Specifically, the acetate and hexanoate salts exist as solids at room temperature, whereas the other four ILs are liquids. This deviation from the commonly reported trend suggests that factors beyond alkyl chain length, including hydrogen-bonding networks, packing efficiency, and ion-pair organization, play a crucial role in determining the physical state of these results by influencing intermolecular interactions and phase behaviour. The principal objective of the present study is to establish comparative-structure property relationships among liquid members of the homologous series, the acetate and hexanoate salts were excluded from the thermodynamic correlations. The ^{1}H and ^{13}C NMR spectra of the ILs are shown in the supporting information (SI) (Figures S3 to S14). The ^{1}H of all the piperazinium-based ILs show the absence of a peak corresponding to the –OH proton of carboxylic acids and show a broad singlet in the region δ 8.5-9.5 ppm corresponding to 2H arising from the hydrogens on the quaternary nitrogen. This confirms the successful synthesis of the PILs. The results of the HRMS characterization investigations are shown in SI in Figures S15 to S20.

The FTIR spectra of the ILs are shown in Figure 3 and Figure S21 for [EtPIPZ][Ace] and [EtPIPZ][Hex]. The ATR-FTIR spectra of the piperazinium-based PILs show asymmetric COO^- stretch in the region between 1550-1610 cm^{-1}. The symmetric COO^- stretch is observed between 1350-1420 cm^{-1}. The aliphatic C-H stretching is observed in between 2850-2950 cm^{-1}, whereas the N-H stretch from piperazinium cation is observed in between 3000-3100 cm^{-1}, and the C-N stretch from the piperazine backbone is observed in between 1200-1330 cm^{-1}. The absence of broad band in the 3200-3600 cm^{-1} region that corresponds to –OH from carboxylic acid also confirms the successful formation of the

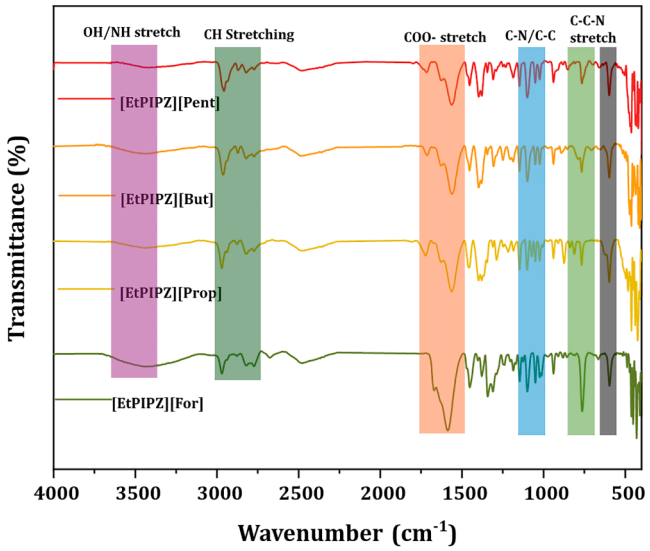

Figure 3. FTIR spectra of EtPIPZ-based ILs.

PILs.

The UV-Vis spectra of the EtPIPZ-based ILs are presented in Figure S22 and S23, with Figure S22 showing [EtPIPZ][Ace] and [EtPIPZ][Hex] and Figure S23 showing [EtPIPZ][For]-[EtPIPZ][Pent]. The spectra do not reveal any distinct absorption bands in the visible region, possibly due to the absence of extended π-conjugation in the saturated piperazine ring, resulting in no significant π-π* transitions. The weak absorption bands in the deep UV region may likely be associated with localized electronic transitions.

3.1. Thermal gravimetric analysis (TGA) and differential scanning calorimetry (DSC)

Thermal Gravimetric analysis is an important technique to elucidate the thermal stability and the decomposition behaviour of the materials under investigation. The TGA profiles of the EtPIPZ-based ILs are shown in Figure 4 and Figure S24 for [EtPIPZ][Ace] and [EtPIPZ][Hex]. The onset temperature (T_{onset}) is the temperature at which decomposition begins, while T_{peak} denotes the temperature at which the maximum rate of decomposition occurs. No significant weight loss is observed below 423.15 K, indicating minimal moisture content and high purity of the synthesized ILs. Among the studied systems, [EtPIPZ][Hex] exhibited the highest thermal stability with a T_{onset} of 593.15 K and T_{peak} above 469.15 K. In general, the T_{onset} for all the other ILs is below 471.15 K. A gradual mass loss of approximately 18-25% was observed in the temperature range 471.15 K- 563.15 K, followed by major decomposition beyond 573.15 K. The thermal stability of the synthesized ILs is not governed by the length of the alkyl chains, indicating that the decomposition behaviour is influenced by multiple structural and intermolecular factors rather than solely the chain length.

The DSC thermograms of the synthesized EtPIPZ-based ionic liquids are presented in Figures 5 and Figure S25 for [EtPIPZ] [Ace] and [EtPIPZ][Hex]. In all samples, a thermal event is observed in the low-temperature region around −58 °C, corresponding to the glass transition temperature (Tg). The absence of sharp melting peaks in this region confirms the predominantly amorphous nature of the ILs. For [EtPIPZ][For], [EtPIPZ][Prop], and [EtPIPZ][But], no distinct crystallization or melting transitions were observed over the studied temperature range, indicating that these systems remain largely amorphous upon heating. Similarly, [EtPIPZ][Ace] exhibits only a glass transition without any clear melting peak, suggesting a highly disordered structure. In contrast, ILs containing larger alkyl chain anions exhibit subtle differences in thermal behaviour. [EtPIPZ][Pent] exhibits an exothermic feature near

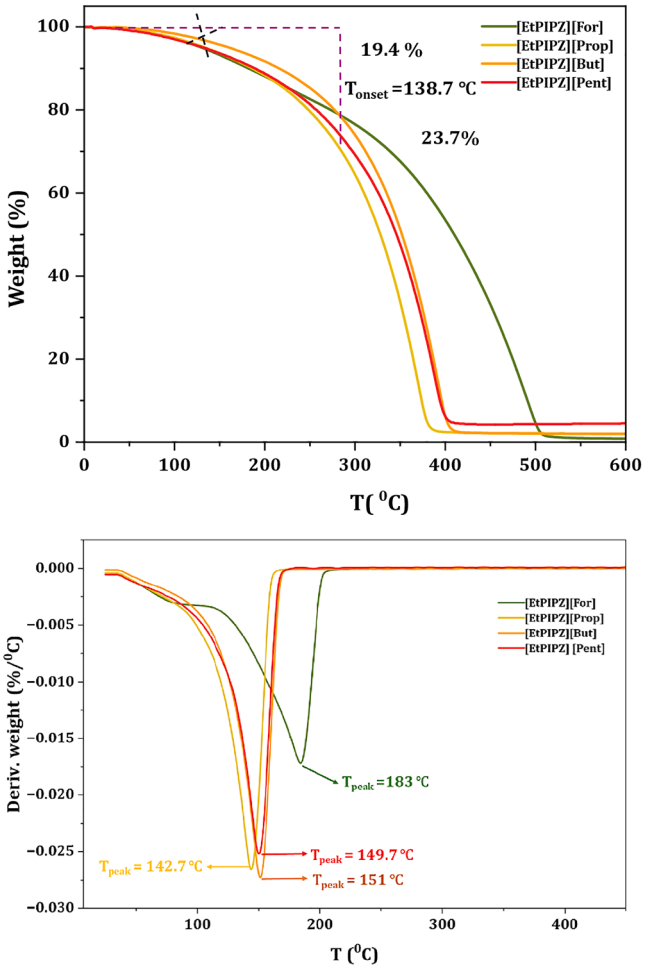

Figure 4. Thermal decomposition of EtPIPZ-based ILs.

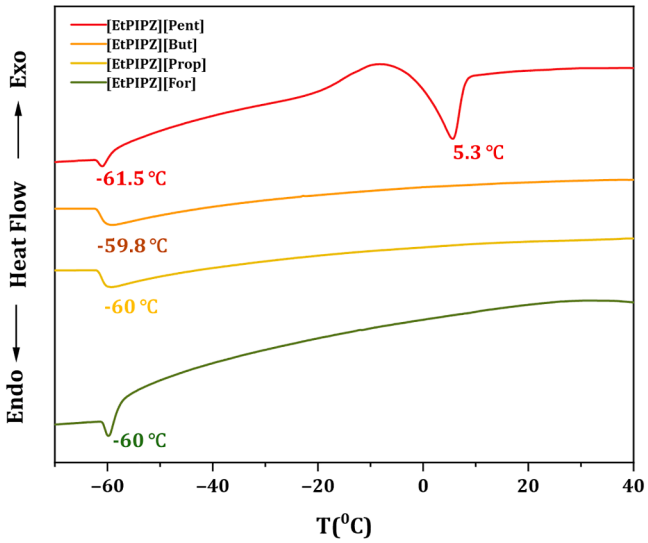

Figure 5. DSC Curve of EtPIPZ-based solid ILs.

5 °C, which may be attributed to cold crystallization, indicating partial structural ordering upon heating. Furthermore, [EtPIPZ][Hex] displays a distinct endothermic peak around 35-40 °C, which can be assigned to a melting transition, suggesting the presence of partial crystallinity. The appearance of such transitions in the longer-chain systems may be

associated with enhanced van der Waals interactions and improved molecular packing. The interruption of the expected liquid-state progression of the ILs by the solid acetate and hexanoate analogues distinguishes the piperazinium based ILs from other homologous ionic liquid systems and indicates that phase behaviour in N-ethylpiperazinium carboxylates is governed by a more complex interplay between molecular structure and intermolecular interactions.

3.2. Density

Density measurements are essential for understanding the intermolecular interactions and structural organization in ILs. The densities of the synthesized EtPIPZ-based RTILs were measured over the temperature range of 293.15-323.15 K at 0.1 MPa. The plot variation of density versus temperature for the ILs is shown in Figure 6. The obtained density values lie in the range 959.6 to 1044.6 kg.m^{-3} as shown in Table S1.

The density of the EtPIPZ-based ILs is found to decrease with an increase in the alkyl chain length of the carboxylate anion and with an increase in the temperature. The density is thus highest for [EtPIPZ][For] and lowest for [EtPIPZ][Pent]. This decrease can be attributed to the increase in molar volume arising from the expansion of the nonpolar region of the anion. As the alkyl chain length increases, the intermolecular hydrogen bonding interactions within the IL system are weakened, resulting in an increase in the free volume. The decrease in density with an increase in temperature is attributed to the thermal expansion and the consequent increase in molar volume. These trends are consistent with previously reported literature for structurally related ionic liquids[35–37]. .Density measurements were performed in triplicate at each temperature, and the corresponding average values are reported in Table S1. The experimental standard deviation (SD) of the density measurements ranged from 0.05 to 0.09 kg.m^{-3} The standard uncertainty of the Anton par DSA 5000M density meter was ±0.005 kg.m^{-3}. Combined standard uncertainties was calculated using the law of propagation of uncertainty by considering both experimental standard deviation and the instrumental uncertainty, Error bars corresponding to ± SD (n=3) have been included in the Figure 6. statistical analysis of the fitted density correlations was performed by linear regression and the corresponding R^2 values and Confidence Interval (CI) are included in Table S2.

The thermal expansion coefficient values computed using experimental density are useful to get insights into the intermolecular interactions. The relation between the density and thermal expansion coefficient is given below in equation (1) [38,39].

$$\alpha = -\frac{1}{\rho}\left(\frac{\partial \rho}{\partial T}\right)_p \quad (1)$$

The plot of thermal expansion coefficient against temperature for the four EtPIPZ-based ILs is given in Figure 7, and the corresponding values are given in Table S3. The values were found to be in the range of 7-8.1 × 10^4 K^{-1} and the corresponding average values derived from the three independent measurements values are reported in Table S3. It increases with the alkyl chain length of the synthesised EtPIPZ-based ILs. The thermal expansion coefficient increases with temperature, which is due to a reduction in density with increasing alkyl chain length in ILs. It can be attributed to an increase in intermolecular interactions and volumetric expansions with temperature, which is responsible for the increase in thermal expansion coefficient[40].

The thermal expansion coefficients of the synthesised N-ethylpiperazinium carboxylate PILs fall within the range generally reported for carboxylate based PILs. A slight increase in thermal expansion coefficient (α) with increasing alkyl chain length, indicates that the incorporation of longer alkyl substituents reduces packing efficiency and enhances molecular mobility, resulting in a greater increase in volume with increasing temperature. This trend is consistent with previous studies on ammonium, pyrrolidinium, and DBU based PILs, where longer alkyl chains weaken intermolecular interactions and facilitate thermal expansion [41–44]. Therefore, the close agreement between the present values and the reported in literature values confirms that the synthesised PILs exhibit characteristic thermal expansion behaviour for this class of ILs.

The uncertainty of the thermal expansion coefficient was calculated using law of prorogation of uncertainty by considering the uncertainties associated with the density measurements at different temperatures. Linear regression analysis was performed to evaluate the temperature dependence of density for each PIL, and the quality of the fit was assessed using the coefficient of determination (R^2). The corresponding confidence interval (CI) values are reported in Table S4.

Apart from the thermal expansion coefficient, other parameters that are crucial to get detailed insights into the ILs are molecular volume (V) and standard entropy (S^0), etc. These parameters can also be calculated from the experimental density data by using equations (2) and (3)[45,46].

$$V = \frac{M}{N_A \cdot \rho} \quad (2)$$

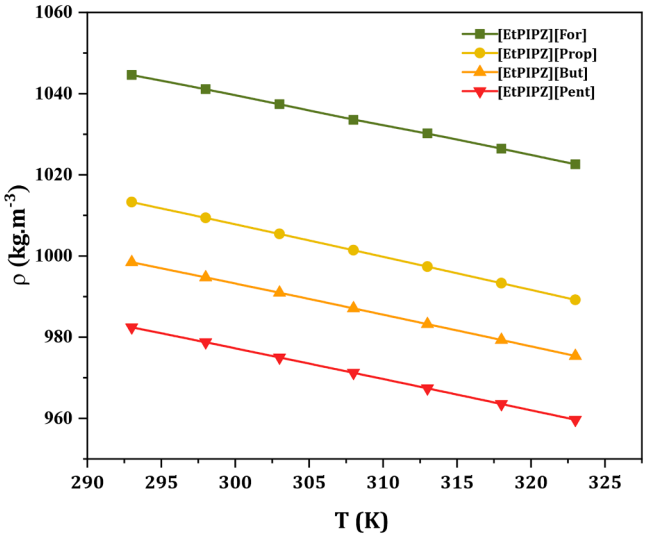

Figure 6. Density of EtPIPZ-based ILs (Standard uncertainties in density $u(\rho)$ = 0.05 kg.m^{-3}).

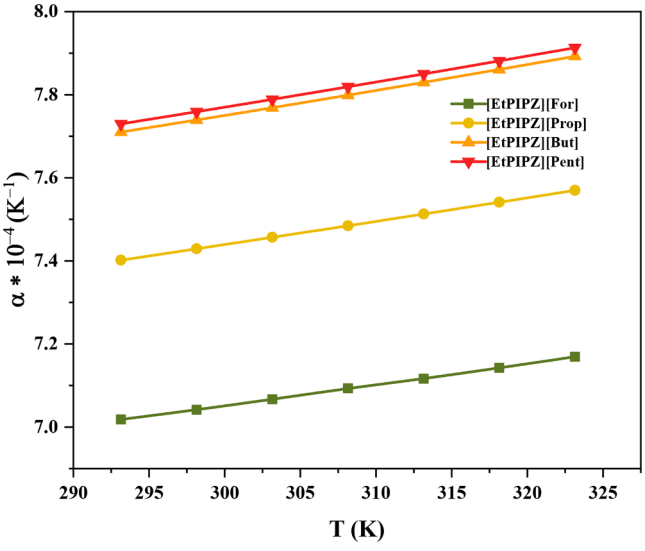

Figure 7. Thermal expansion coefficient of EtPIPZ-based ILs (Standard uncertainties in thermal expansion coefficient $u(\alpha)$ = 0.005 × 10^{-4} K^{-1}).

$$S^0\left(J.K^{-1}.mol^{-1}\right) = 1246.5V\ \left(nm^3\right) + 29.5 \quad (3)$$

Where V is the molecular volume (nm^3) of the EtPIPZ ILs, M is the molecular weight ($g.mol^{-1}$), N_A is the Avogadro number (6.02×10^{23} mol^{-1}), and ρ is the density ($kg.m^{-3}$). The plot of molecular volume V (nm^3) of EtPIPZ-based ILs against temperature is given in Figure 8, and the corresponding data is given in Table S5. The values of V were found to be in the range 0.253-0.374 nm^3. The value of V increases with an increase in the length of the alkyl chain of the carboxylate anion and increases with an increase in temperature for each IL[47,48]. Thus, the increasing order of molecular volume of EtPIPZ-based ILs can be represented as [EtPIPZ][For] < [EtPIPZ][Prop] < [EtPIPZ][But] < [EtPIPZ][Pent]. This behaviour can be due to the thermal expansion, as an increase in temperature increases the molecular kinetic energy, resulting in greater intermolecular separation and an overall increase in free volume.

The molecular volume was calculated as a function of the number of carbon atoms in the anionic alkyl chain and is presented in Figure 9. The standard deviation (SD) was calculated from the corresponding molecular volume data. The uncertainty in the molecular volume was estimated using the law of propagation of uncertainty based on the experimental density measurements. The SD was observed in the range of 0.0001 nm^3, while the standard error (SE) was approximately 0.00006 nm^3, with a corresponding CI of ± 0.000253 nm^3 .In addition, linear regression analysis was performed to evaluate the fitted correlations and the corresponding coefficients of determination (R^2) and CI values are reported in Table S6 and strong linear correlation (R^2=0.99) was observed between molecular volume and number of carbon atoms in anionic site, which is described by the equation: V (nm^3) = 0.0297n_c + 0.182, where n_c represents the number of carbon atoms in the anion. The slope value of 0.0297 nm^3 indicates the incremental contribution of each methylene (–CH_2–) group to the molecular volume of the ionic liquid. This contribution is consistent with the reported volume of –CH_2– groups as a function of the number of carbons in carboxylate anion chain lengths [49,50]. The results clearly indicate that molecular volume increases systematically with increasing alkyl chain length. Consequently, [EtPIPZ][Pent] occupies a larger volume compared to ILs containing shorter alkyl chain anions.

The standard entropy (S^o) values were estimated using an empirical correlation based on the molecular volume (nm^3) (equation 3) rather than direct calorimetric measurements, following the approach proposed by Panda[51]. Such empirical correlations have been widely

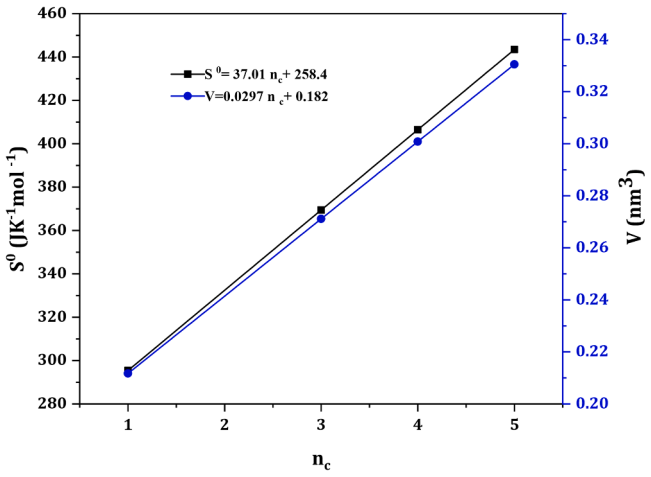

Figure 9. Standard entropy of EtPIPZ-based ILs.

applied to ILs and provide reliable comparative estimates despite their inherent approximations. Nevertheless, some deviations may arise from molecular flexibility, hydrogen-bonding interactions and ion-specific effects that are not explicitly considered in the empirical model. The values were estimated at different temperatures of 293.15K-323.15K for EtPIPZ-based ILs. The calculated values are presented in Figure 10 and summarised in Table S7. The value of standard entropy (S^o) was found to fall in the range of 345.23-496.46 $J.K^{-1}.mol^{-1}$. This plot indicates that standard entropy increases with increasing alkyl chain length and with increasing temperature.

The experimental precision was evaluated using standard deviation (SD), standard error (SE) and confidence interval (CI) based on three independent measurements (n=3). The calculated values were SD = 0.10 J $K^{-1}.mol^{-1}$, SE =0.05 J $K^{-1}.mol^{-1}$, CI is ±0.25 J $K^{-1}.mol^{-1}$, The standard uncertainty, estimated using the law of propagation of uncertainty, was 0.05 J $K^{-1}.mol^{-1}$ .In addition, statistical analysis of the standard entropy correlation was performed using linear regression and the corresponding coefficient of determination (R^2) and CI values are reported in the Table S8.

To get insights into the relative stability and strength of ions in the synthesised EtPIPZ-based ILs, the lattice potential energy (U_{POT}) was calculated using Glasser's theory, assuming ILs behave as MX-type salts, according to equations (4) and (5)[52,53].

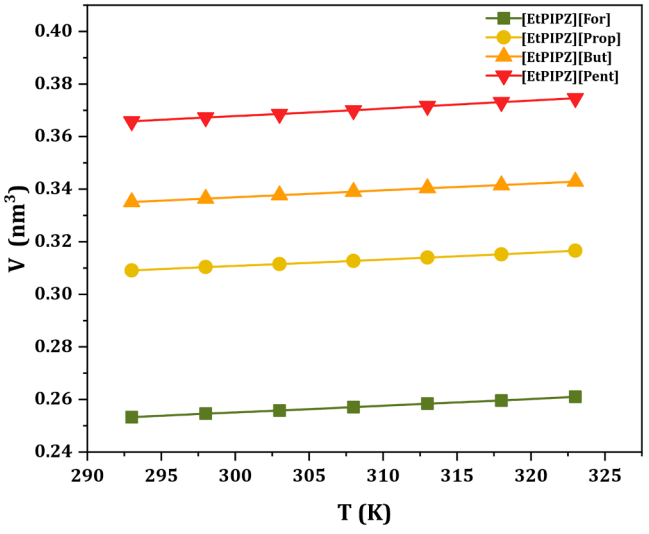

Figure 8. Molecular Volume of EtPIPZ-based ILs (Standard uncertainties in molecular volume $u(V)$ = 0.0003 nm^3).

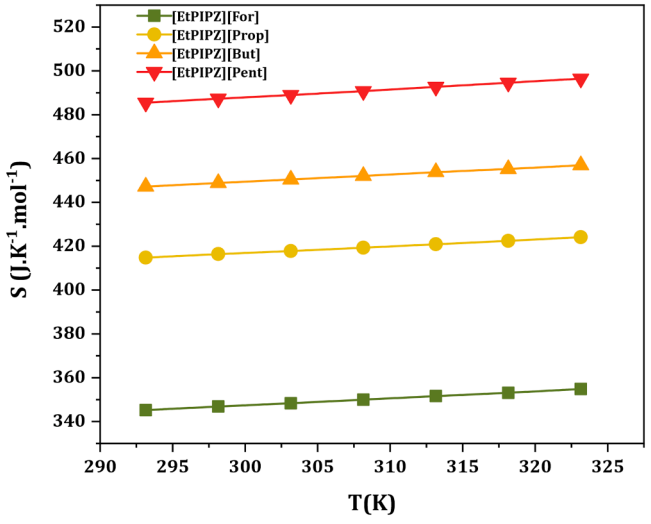

Figure 10. Standard entropy of EtPIPZ-based ILs (Standard uncertainty of u (S^0) = 0.05 $J.K^{-1}.mol^{-1}$).

$$U_{POT}\ \ (kJ.mol^{-1}) = 1981.2\left(\frac{\rho}{M}\right)^{\frac{1}{3}} + 103.8 \quad (4)$$

$$V_m^* = V_c^* + V_a^* \quad (5)$$

The calculated lattice potential energy (LPE) values are shown in Figure 11 and listed in Table S9, ranging from 570.9 to 513.9 kJ.mol^{-1}. LPE primarily depends on the electrostatic interactions between ions and is inversely related to the molar volume. The molar volume (V_m^*) is the sum of the molecular volumes of the cation (V_c^*) and anion (V_a^*) as proposed by Esperanca[54]. As the alkyl chain length of the anion increases, the anionic volume increases, leading to a larger overall molar volume and consequently lower lattice potential energy. The decrease in LPE with increasing alkyl chain length indicates reduced packing efficiency, increased free volume, and higher standard entropy in the EtPIPZ-based ILs. The calculated LPE values are all below 575 kJ.mol^{-1}, which is lower than that of inorganic fused cesium iodide (CsI), whose LPE is 613 kJ.mol^{-1}. These comparatively lower LPE values confirm the liquid nature of the synthesized ionic liquids [41,55]. The experimental precision was evaluated using the standard deviation (SD), standard error (SE), and confidence interval (CI) based on three independent measurements (n=3). The calculated values were SD = 0.1 kJ mol^{-1}, SE =0.05 kJ mol^{-1}, CI is ±0.25 kJ mol^{-1}, The standard uncertainty, estimated using the law of propagation of uncertainty, was 0.05 kJ mol^{-1}. In addition, the statistical analysis of the lattice energy potential correlation was performed using linear regression, and the corresponding coefficient of determination (R^2) and CI values are provided in Table S9. Although the empirical approach proposed by Glasser has been widely employed for ionic liquids, it possesses certain limitations, particularly for protic ionic liquids, where strong hydrogen bonding and directional ion-ion interactions may not be fully represented by empirical volume-based models[43]. Therefore, the calculated lattice potential energies should be interpreted as approximate comparative values rather than absolute thermodynamic quantities. However, as all investigated compounds belong to the same homologous family and were analyzed using an identical methodology, the calculated values remain useful for evaluating relative trends across the series rather than an exact quantitative description of crystal lattice stabilization[41].

3.3. Speed of sound

The speed of sound is an important parameter for analysing the physicochemical properties of synthesised ILs. It is defined as the distance travelled per unit time by a sound wave propagating through an elastic medium[56–58]. The speed of sound is generally expressed in meters per second (m.s^{-1}). The speed of sound for the synthesized ILs was measured by using an Anton Paar Density and Sound Velocity Meter (DSM 5000 M), equipped with a circular cell with dimensions of 8 mm diameter and 5 mm depth. The measurements were performed in the temperature range of 293.15-323.15 K at 0.1 MPa. The plot of speed of sound (u) versus temperature for EtPIPZ-based ILs is shown in Figure 12. The speed of sound data was found to be in the range of 1349-1602 m.s^{-1} and the corresponding data was represented in Table S10.

Insights into the data reveal that the speed of sound (u) decreases with an increase in the alkyl chain length of anions in EtPIPZ-based ILs and decreases with an increase in temperature. High speed of sound values are indicative of a more closely packed structure, whereas lower values suggest less compact packing. The same pattern is observed in the present case, with [EtPIPZ][For] having the highest speed of sound value compared to the other three ILs. The decrease in speed of sound at higher alkyl chain lengths implies increased free space within the system, which is consistent with the literature reports[59–61]. The experimental precision was evaluated using standard deviation (SD), standard error (SE) and confidence of interval (CI) based on three independent measurements (n=3). The calculated values were SD = 0.1 m s^{-1}, SE =0.05 m s^{-1}, CI is ±0.25 m s^{-1} . The standard uncertainty, estimated using the law of propagation of uncertainty, was 0.05 m. s^{-1}. In addition, the statistical analysis of the speed of sound correlation were performed using linear regression, and the corresponding coefficient of determination (R^2) and CI values are reported in Table S11.

Isentropic compressibility (β_s) is an important thermodynamic property that can be calculated by using experimental density (ρ) and speed of sound (u) with the help of the Newton-Laplace Equation (6) given below[62].

$$\beta_s = \frac{1}{\rho u^2} \quad (6)$$

Isentropic compressibility (β_s) is a useful parameter used to analyse the free space available in ILs. The plot of β_s versus temperature for EtPIPZ-based ILs is shown in Figure 13, and the data are summarized in Table S12. The values lie in the range 372-572 TPa^{-1}. The value of isentropic compressibility (β_s) was found to increase with an increase in the length of the alkyl chain of the anion and with the increase in temperature[63–65]. Higher β_s value in [EtPIPZ][Pent] indicate a partially packed structure with greater free space within the ILs. Similar behaviour has been reported by Capleo et al. for ammonium

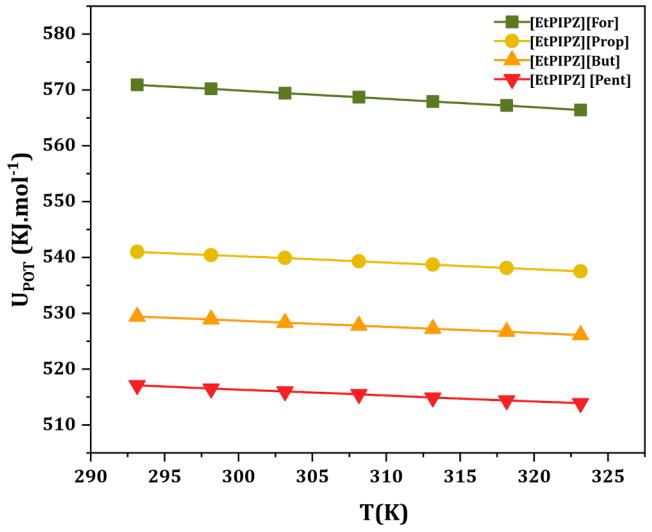

Figure 11. Lattice energy potential of EtPIPZ-based ILs (Standard uncertainties in lattice potential $u(U_{POT})$ = 0.05 kJ.mol^{-1}).

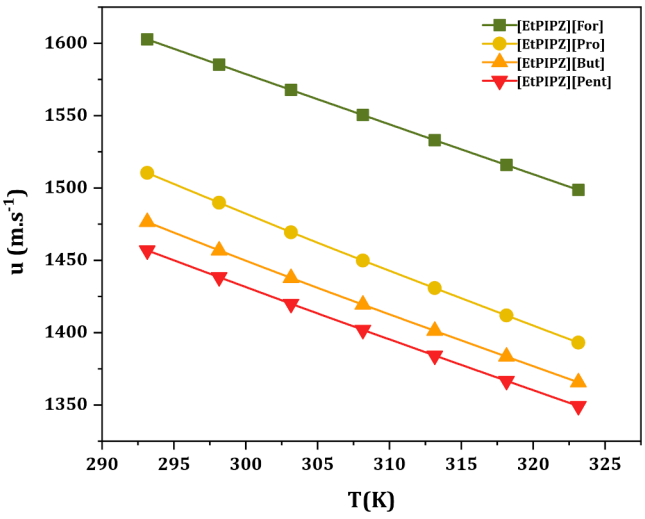

Figure 12. Speed of sound of EtPIPZ-based ILs (Standard uncertainties in sound velocity $u(u)$ = 0.05 m. s^{-1}).

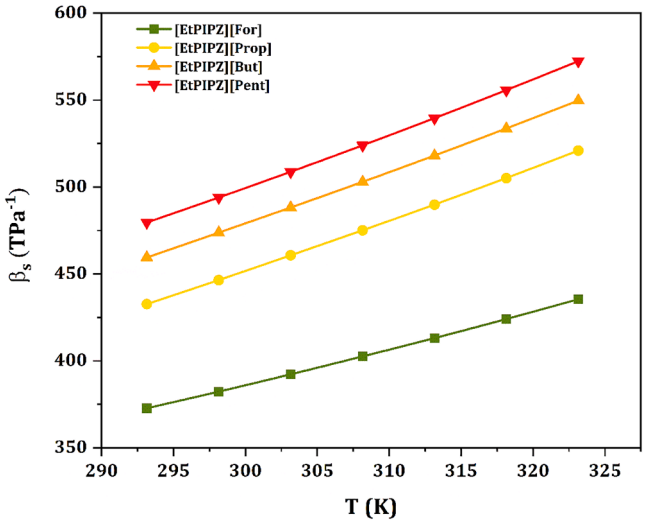

Figure 13. Isentropic compressibility of EtPIPZ-based ILs (Standard uncertainties in isentropic compressibility $u(\beta s)$ = 0.05 TPa^{-1}).

nitrate-based protic ionic liquids (PILs). The experimental precision was evaluated using the standard deviation (SD), standard error (SE) and the confidence interval (CI) based on three independent measurements (n=3), The calculated values were SD = 0.1 TPa^{-1}, SE =0.05 TPa^{-1}, CI = ±0.25 TPa^{-1}. The standard uncertainty estimated using the law of propagation of uncertainty, was 0.05 TPa^{-1}.

Since isentropic compressibility gives insights into free space availability in ILs, the intermolecular free length (L_f) was further evaluated to get a better understanding of intermolecular interaction in the ILs. Equation (7) is known as Jacobson's empirical relation used for estimating the intermolecular free length (L_f) [66–68].

$$L_f = K_J\sqrt{\beta_s} \tag{7}$$

Where K_J is the temperature-dependent Jacobson constant.

The calculated L_f values for the synthesized EtPIPZ-based ILs are presented in Figure 14, and the corresponding data are listed in Table S13. The values of L_f range from 0.38 to 0.51 Å, indicating the increase of L_f with increasing alkyl chain length of the anions and with increasing temperature [69]. The combined results of isentropic compressibility and intermolecular free length clearly indicate that intermolecular free space increases from [EtPIPZ][For] to [EtPIPZ][Pent] due to an increase in alkyl chain lengths of anions. Furthermore, as temperature increases, enhanced ionic mobility results in greater free volume within the IL system.

The experimental precision was evaluated using the standard deviation (SD), standard error (SE) and the confidence interval (CI), based on the three independent measurements (n=3). The calculated values were SD = 0.0001 Å, SE = 0.00005 Å, CI = ±0.00025 Å. The standard uncertainty, estimated using the law of propagation of uncertainty, was 0.00005 Å

3.4. Refractive index

The refractive index (n_D) of the synthesized EtPIPZ-based ILs was measured using Refracto 30-GS instrument, and temperature was controlled with the help of a Julabo circulating bath to maintain proper temperature intervals. A plot of n_D *versus* T for EtPIPZ-based ILs is shown in Figure 15, and the corresponding data given in Table S14.

The value of n_D for the ILs was found to be in the range 1.43-1.48. It was found that the refractive index decreases with an increase in the alkyl chain length of the carboxylate anion, which may be attributed to the increase in molar volume and free volume associated with the larger anions, which reduces the overall polarizability density of the system. The value of n_D also decreases with an increase in temperature due to thermal expansion and the resulting reduction in density [70,71].

The experimental precision was evaluated using the standard deviation (SD), standard error (SE), and the confidence interval (CI), based on three independent measurements (n=3). The calculated values were SD = 0.0001, SE =0.00005, CI is ±0.00025. The standard uncertainty, estimated using the of law of propagation of uncertainty, was 0.00005. In addition, the statistical analysis of the speed of sound correlation was performed using linear regression, and the corresponding coefficient of determination (R^2) and CI values are provided in Table S15.

A linear relation between refractive index and temperature was established by employing equation (8) given below[72,73].

$$n_D = A_O + A_1 T \tag{8}$$

Where A_0 and A_1 are correlation coefficients, whose values are shown in the Table S15. The obtained values show an excellent fit to the linear equation, with R^2 values greater than 0.99, and the standard deviation values were found to be about 0.00005 for the synthesised EtPIPZ-based ILs, indicating high precision of the experimental measurements.

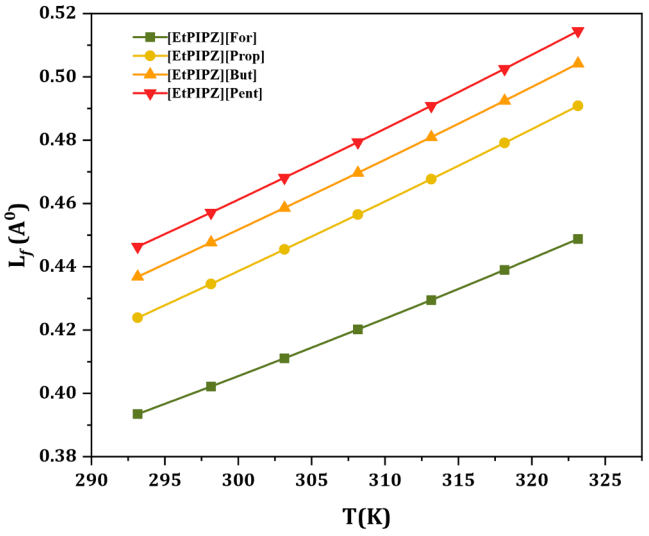

Figure 14. Intermolecular free volume of EtPIPZ-based ILs, (Standard uncertainties in intermolecular free volume $u(L_f)$ = 0.00005 Å).

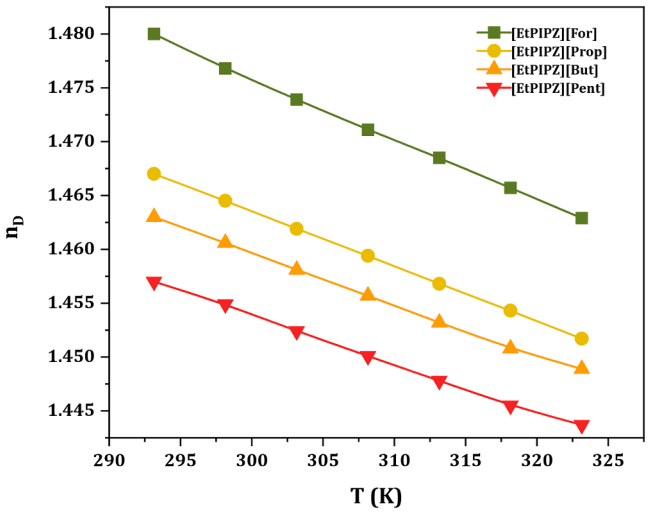

Figure 15. : Refractive index of EtPIPZ-based ILs (Standard uncertainties in refractive index u (n_D) = 0.00005).

The experimental refractive index data were further correlated with the density data to compute another important thermodynamic parameter, i.e., molar refraction (R_m). It can be calculated using the Lorentz-Lorenz equation given in equation (9). The molar refraction (R_m) is useful for correlating the physicochemical properties such as density, surface tension, and polarizability[74,75].

$$R_m = \left(\frac{n_D^2 - 1}{n_D^2 + 2}\right)\frac{M}{\rho} = \frac{4N_A\alpha_e}{3\epsilon^0} \quad (9)$$

Where R_m is the molar refraction ($cm^3.mol^{-1}$), n_D is the refractive index, M is the molecular weight ($g.mol^{-1}$), ρ is the density ($g.cm^{-3}$), N_A is Avagadro's number (mol^{-1}), α_e is the molecular polarizability and ϵ^0 is the permittivity in the vacuum. The plot of molar refraction (R_m) versus temperature for EtPIPZ-based ILs is shown in Figure 16, and the resulting data are presented in Table S16. The R_m values increase with an increase in alkyl chain length of anions and decrease statistically with temperature, which is due to static polarizability, which is caused by van der Waals dispersion forces of ILs[76]. The experimental precision was evaluated using the standard deviation (SD), standard error (SE) and confidence interval (CI) based on three independent measurements (n=3). The calculated values were SD = 0.01 $cm^3\ mol^{-1}$, SE =0.005 $cm^3\ mol^{-1}$, CI is ±0.00025 $cm^3\ mol^{-1}$. The standard uncertainty, estimated using the law of propagation of uncertainty, was 0.005 $cm^3\ mol^{-1}$.

Molar Refraction data can be used to calculate the molecular free volume (V*f*) of ILs by using equation 10 as shown below, based on the assumption that the ILs are hard spheres [77].

$$V_f = V_m^* - R_m \quad (10)$$

Where, V_m^* is the molar volume. The plot of the molecular free volume (V_f) against temperature for the synthesized ILs is given in Figure 17, and the corresponding data is given in Table S17. The values of V_f were found to be in the 108.7-164.7 × 10^{-6} $m^3.mol^{-1}$.

The results make it evident that V_f increases with an increase in alkyl chain length of the anions, and also increases with an increase in temperature. The obtained free volume data are in good agreement with the molecular free length (L*f*) and the speed of sound values, as discussed in the previous section. Free volume increased with increasing alkyl chain length, indicating reduced ion packing efficiency and enhanced structural flexibility. This behaviour arises from the incorporation of longer alkyl chains, which increase the unoccupied space within the liquid structure and weaken the intermolecular packing. Similar trends have been reported for ammonium, pyrrolidinium and DBU based PILs.

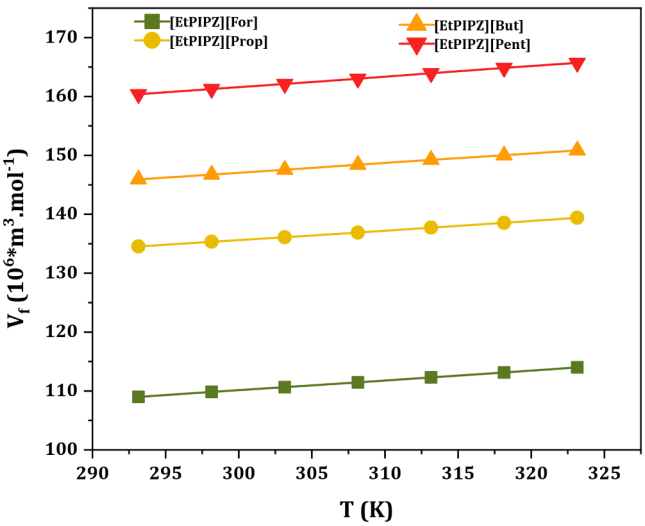

Figure 17. Free volume (V_f) of EtPIPZ-based ILs (Standard uncertainties in free volume $u(V_f)$ 0.005 $m^3.mol^{-1}$).

Therefore, the present results are consistent with the established structure property relationships observed for related PIL systems[41–43,51].

The experimental precision was evaluated by using the standard deviation (SD), standard error (SE) and confidence (CI) based on three independent measurements (n=3). The calculated values were SD = 0.01 × 10^{-6} $m^3\ mol^{-1}$, SE =0.005 × 10^{-6} $m^3\ mol^{-1}$, CI is ±0.025 × 10^{-6} $m^3\ mol^{-1}$. The standard uncertainty, estimated using the law of propagation of uncertainty, was 0.005 × 10^{-6} $m^3\ mol^{-1}$.

3.5. Viscosity

Viscosity (η) is an important transport property that governs mass transfer in liquids and ILs. In IL systems, viscosity is primarily influenced by hydrogen bonding, dispersion forces, and Coulombic interactions[78,79]. The dynamic viscosities of the synthesised EtPIPZ-based ILs were measured over the temperature range of 293.15K -323.15 K, and the results are presented in Figure 18, with the corresponding data summarized in Table S18.

The measured viscosity values lie in the range 53.5-303 mPa.s. The viscosity of EtPIPZ-based ILs follows the decreasing order: [EtPIPZ]

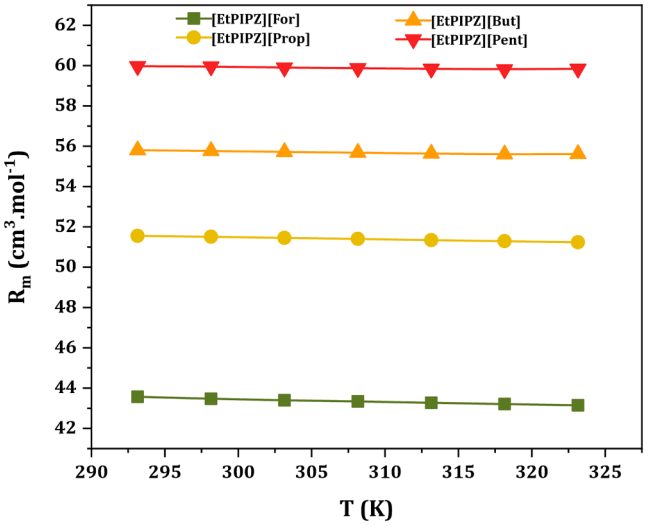

Figure 16. Molar refraction (R_m) of EtPIPZ-based ILs. (Standard uncertainties in molar refraction $u(nR_m)$ = 0.005 $cm^3\ mol^{-1}$).

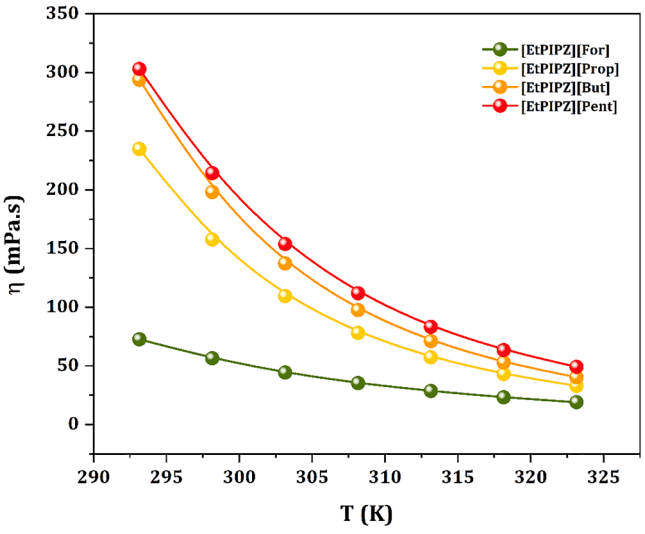

Figure 18. Viscosity of EtPIPZ-based ILs (Standard uncertainties viscosity $u(\eta)$ = 0.11 mPa.s).

[For]< [EtPIPZ][Prop]< [EtPIPZ][But]<[EtPIPZ][Pent] as shown in Figure 18. For the propanoate, butanoate, and pentanoate derivatives, the observed increase in viscosity with increasing alkyl chain length of the anion may be attributed to the relative weakening of strong Coulombic and hydrogen-bonding interactions due to increased steric bulk and free volume. Although dispersion forces increase with chain length, their contribution does not compensate for the reduced electrostatic interactions, leading to an overall increase in viscosity. An important outcome of this study is that the transport properties of N-ethyl piperazinium carboxylate ILs are significantly influenced by the alkyl chain length of carboxylate anion. The viscosity increases progressively from [EtPIPZ][For] to [EtPIPZ][Pent] indicating that longer alkyl chains strengthen intermolecular interactions and hinder ion mobility. These findings demonstrate that systematic modification of the anion structure provides an effective approach for tailoring the transport properties. The increase in viscosity with increasing temperature can be attributed to enhanced molecular motion and partial disruption of intermolecular interactions between the ions.

The experimental precision was evaluated using the standard deviation (SD), standard error (SE), and confidence interval (CI) based on three independent measurements (n=3). The calculated values were SD = 0.18 mPa.s, SE = 0.11 mPa.s, CI = ±0.44 mPa.s. The standard uncertainty, estimated using law of propagation of uncertainty, was 0.11 mPa.s.

The activation energy for viscous flow (E_η) can be determined by using the Arrhenius equation (11)[80,81].

$$\ln\eta = \ln\eta_\infty + \frac{E_\eta}{RT} \tag{11}$$

Where η is the dynamic viscosity, η_∞ is the viscosity at infinite temperature, E_η is the activation energy, R is the universal gas constant, and T is the temperature in K and $\ln\eta$ versus 1/T plot represented in Figure 19, The experimental precision was evaluated using the standard deviation (SD), standard error (SE), and confidence interval (CI) based on three independent measurements (n=3). The calculated values were SD = 0.01, SE = 0.005, CI = ±0.025. The standard uncertainty, estimated using the law of propagation of uncertainty, was 0.005. the corresponding data shown in Table S19. The activation energy E_η is calculated from the experimental dynamic viscosity data, and the data is shown in Table 3.

E_η is the minimum energy barrier that must be overcome for ion movement within the IL system. The $\ln\eta$ versus 1/T plots, shows that activation energy for EtPIPZ-based ILs initially increases, followed by a decrease with the increasing alkyl chain length of anions in EtPIPZ-based ILs. This trend matches the trend of the experimental dynamic viscosity[82].

Table 3
Activation energy and ln η_∞ values of EtPIPZ-based ILs as a function of viscosity.

ILs	Slope= $\frac{E_\eta}{RT}$	$\ln\eta_\infty$	E_η =(kJ.mol^{-1}.)	R^2
[EtPIPZ][For]	4219.25	-10.11	35.07	0.99
[EtPIPZ][Prop],	6197.10	-15.72	51.52	0.99
[EtPIPZ][But],	6274.86	-15.75	52.16	0.99
[EtPIPZ][Pent]	5763.17	-13.96	47.91	0.99

3.6. Ionic conductivity

The determination of ionic conductivity (σ)is essential for evaluating the physicochemical properties of ILs, considering their potential applications as electrolytes in the domain of energy storage systems [83–86]. In general, the conductivity of ILs is lower than that of conventional inorganic salts. This can be attributed to the higher viscosity of the ILs and, consequently, the reduced movement of ions[87]. The experimentally determined values of ionic conductivity (σ) for EtPIPZ-based ILs as a function of temperature are given in Table S20, and the plot of the same is given in Figure 20.

The value of ionic conductivity (σ) was found to be in the range 0.11-4.11 mS/cm. It is evident from the results that the synthesized EtPIPZ-based ILs exhibit relatively higher viscosity, leading to moderate to low ionic conductivity. Furthermore, ionic conductivity decreases with a corresponding increase in the alkyl chain length of the carboxylate anion due to increased volume contribution of additional methyl groups that lead to enhanced van der Waals interactions and viscosity. The increase in viscosity reduces the ion mobility and reduces the free volume available for ion transportation[88,89]. The ionic conductivity increases with an increase in temperature.

The experimental precision was evaluated using the standard deviation (SD), standard error (SE), and confidence interval (CI) based on three independent measurements (n=3). The calculated values were SD = 0.003 mS cm^{-1}, SE = 0.002 mS cm^{-1}, CI = ±0.007 mS cm^{-1}. Standard uncertainty, estimated using the law of propagation of uncertainty, was found to be 0.002 mS cm^{-1}.

Furthermore, the temperature dependence of ionic conductivity (σ) was fitted using the Arrhenius equation in its logarithmic form, as

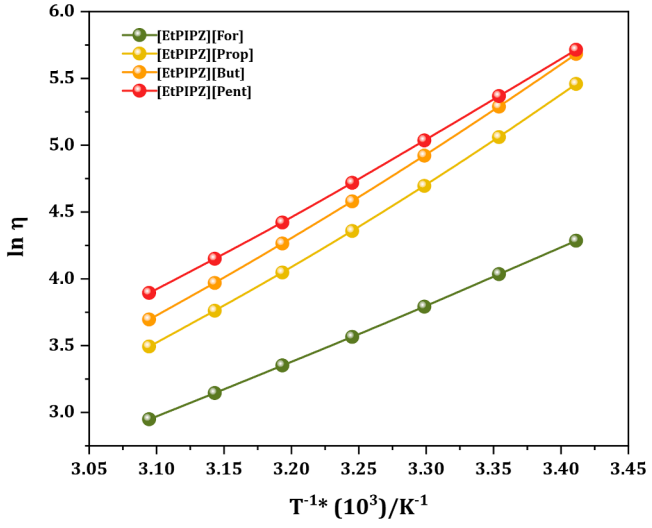

Figure 19. Arrhenius plot of EtPIPZ-based ILs. (Standard uncertainties activation energy $u(\ln\eta)$ = 0.005).

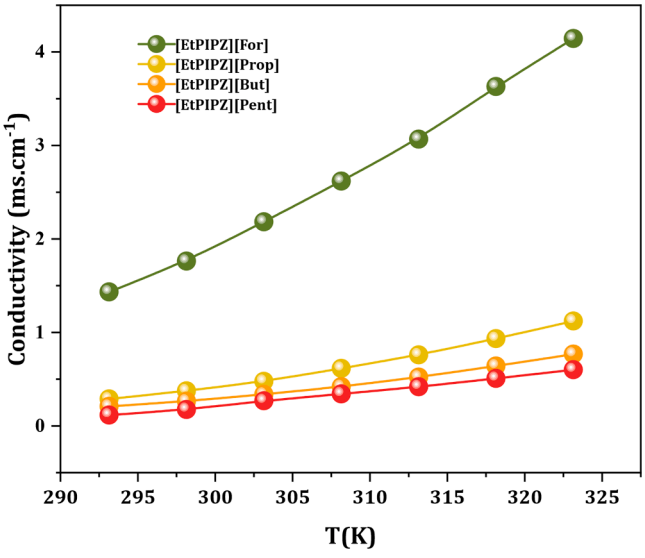

Figure 20. Conductivity of EtPIPZ-based ILs (Standard uncertainties in conductivity $u(\sigma)$ = 0.002 mS.cm^{-1}).

given below in equation (12)[90,91].

$$\ln\sigma = ln\sigma_0 - \frac{E_a}{RT} \quad (12)$$

Where R is the universal gas constant, E_a is the activation energy for ILs in logarithmic form of the Arrhenius equation, T is absolute temperature, and $ln\sigma_0$ is the constant, presented in Table 4. The fitted plots of lnσ versus 1/T (K^{-1}) for EtPIPZ-based ILs are presented in Figure 21. The corresponding data is summarised in Table S21.

A good linear correlation was obtained for all the ILs, with correlation coefficients (R^2) greater than 0.99. This confirms the applicability of the Arrhenius model within the studied temperature range. The activation energy was calculated from the slope of the $ln\sigma_0$ versus 1/T plots and was found to lie in the range of 28.01-37.53 kJ.mol^{-1} and calculated data represented in Table S21. Among the four ILs, [EtPIPZ][Pent] exhibited the highest activation energy, indicating the greatest resistance to ion movement. This indicates that it has higher viscosity and lower conductivity when compared with [EtPIPZ][But], [EtPIPZ][Prop], and [EtPIPZ][For].

The experimental precision was evaluated using the standard deviation (SD), standard error (SE) and confidence interval (CI) based on three independent measurements (n=3). The calculated values were SD = 0.01, SE = 0.005, CI = ±0.025. The standard uncertainty, estimated using the law of propagation of uncertainty, was 0. 005.

3.7. DFT analysis

DFT analysis was performed on the synthesised ILs, viz. [EtPIPZ][For], [EtPIPZ][Prop], [EtPIPZ][But], and [EtPIPZ][Pent]. The geometries of the ILs were optimised by using the B3LYP functional and 6-311 ++ G (d, p) basis set. The obtained optimised geometries are illustrated in Figure 22. The ILs were formed via the proton transfer from the acidic –OH of carboxylic acid to the nitrogen of amine, resulting in the cationic and anionic parts of the PILs. The electrostatic interactions between oppositely charged ions in PILs, along with poor packing efficiency and charge delocalization, prevent the crystallization resulting in RTILs. This ionic bond formed in these PILs between opposite charges, which keeps them Liquid in nature[92,93]. The distance between the cationic and anionic units was found to be 1.696 Å, 1.696 Å, 1.749 Å, and 1.696 Å in [EtPIPZ][For], [EtPIPZ][Prop], [EtPIPZ][But], and [EtPIPZ][Pent], respectively. The optimised structures of [ETPIPZ] ILs, having the maximum binding energies, indicate that the synthesised ILs are more stable, and ions are closely packed together in the system.

The Interaction energy describes the strength of the attractive interactions between the cation and in an IL system. It was calculated using DFT by comparing the electronic energy of the optimised ion pair with the electronic energies of the corresponding isolated cation and anion. The interaction energy of ILs was calculated using equation (13)

$$E_{Int} = E_{IL} - (E_{Cation} + E_{Anion}) \quad (13)$$

The calculated interaction energies are listed in Table 5.

Table 5 presents the interaction energies of the synthesised N-ethylpiperazinium carboxylate PILs calculated using DFT. The results show that the magnitude of the interaction energy decreases with increasing alkyl chain length of the carboxylate anion, indicating a gradual weakening of the cation-anion interactions. Among the investigated

Table 4
Activation Arrhenius plot of EtPIPZ-based ILs as a function of ionic conductivity.

ILs	Slope = $-\frac{E_a}{RT}$	$ln\sigma_0$	E_a(kJ.mol^{-1})	R^2
[EtPIPZ][For]	-3369.25	11.87	28.01	0.99
[EtPIPZ][Prop]	-4318.82	13.50	35.90	0.99
[EtPIPZ][But]	-4431.65	13.51	36.84	0.99
[EtPIPZ][Pent]	-4514.89	13.52	37.53	0.99

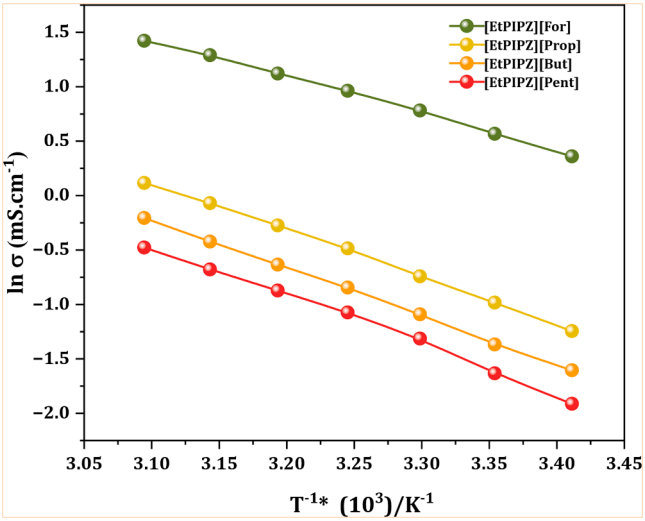

Figure 21. Arrhenius plot of EtPIPZ-based ILs as a function of conductivity. (Standard uncertainties activation energy $u(ln(\sigma)) = 0.005$).

PILs, [EtPIPZ][For] exhibit the most negative interaction energy (-13.74 kcal/mol), indicating the strong attraction between the cation and anion. In contrast, [EtPIPZ][Pent] exhibit the least negative interaction energy (-6.28 kcal/mol), indicating relatively weaker ion-ion interactions. This trend suggests that increasing the alkyl chain length of the carboxylate anion increases the separation between the ions and reduces the strength of the electrostatic attraction. Consequently, the calculated interaction energies provide valuable insights into the relative strength of ion pairing and the stability of the synthesised PILs. To further understand the nature these intermolecular interactions, the interaction energy results were correlated with the reduced density gradient (RDG) analysis, which provides a visual representation of the non-covalent interactions governing the stability of the PILs.

The RDG analysis was performed using Multiwfn, and the corresponding 3D RDG isosurfaces were visualised using VMD. In addition, the non-covalent interaction (NCI) scatter plots of RDG versus sign $(\lambda_2)\rho$ were generated using Gnuplot to identify and characterise the attractive, repulsive and weak van der Waals interactions present in the synthesised PILs.

The RDG scatter plots and the corresponding 3D isosurfaces of the synthesised PILs are presented in Figure 23. In the RDG scatter plots, the negative sign $(\lambda_2)\rho$ region (blue) represents attractive interactions, the region around zero (green) corresponds to weak van der Waals interactions, and the positive sign $(\lambda_2)\rho$ region (red) indicates steric repulsion. A similar interpretation applies to the RDG isosurfaces, where blue isosurfaces represent strong attractive interactions, including hydrogen bonding and electrostatic interactions between the cation and anion, while the green isosurfaces correspond to weak van der Waals interactions. The red regions indicate steric repulsion arising from close atoms contacts[94].

The RDG analysis provides molecular-level evidence for the non-covalent interactions present in the synthesised PILs. Among the investigated compounds, [EtPIPZ][For] exhibits the most prominent blue isosurfaces, indicating stronger attractive interactions between cation and anion, As the alkyl chain length of carboxylate anion increases from formate to pentanoate, the blue isosurface regions gradually decrease, while the green regions associated with weak van der Waals interactions become more prominent as shown in Figure 23.This observation is consistent with the calculated interaction energies, which become less negative with increase in alkyl chain length.[EtPIPZ][For] has higher density and speed of sound, suggesting a more compact liquid structure. However, its comparatively lower viscosity and higher conductivity indicate that ion transport is governed by the combined effects

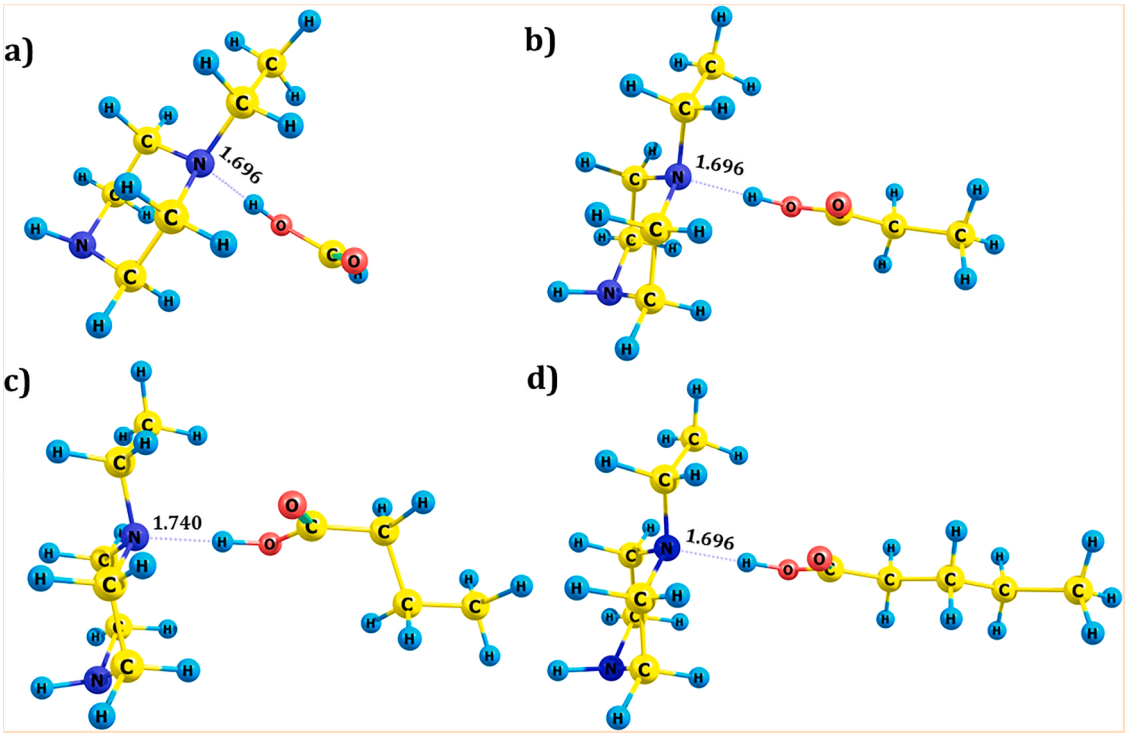

Figure 22. Optimised geometries of a) [EtPIPZ][For], b) [EtPIPZ][Prop], c) EtPIPZ] [But], and [EtPIPZ][Pent].

Table 5
Interaction energies of ILs.

ILs	E_{IL} (kcal/mol)	E_{Cation} (kcal/mol)	E_{anion} (kcal/mol)	I_E (kcal/mol)[a]
[EtPIPZ][For]	-336509.49	-217400.70	-119095.05	-13.74
[EtPIPZ][Prop]	-385830.56	-217400.70	-168417.30	-12.56
[EtPIPZ][But]	-410491.69	-217400.70	-193078.43	-12.56
[EtPIPZ][Pent]	-435146.54	-217400.70	-217739.56	-06.28

[a] Standard computational uncertainty associated with calculated interaction energies is estimated to be ± 3 kcal/mol based on the typical accuracy of DFT methods for molecular interaction energies.

of intermolecular interactions, molecular structure and ion mobility, rather than interaction energy alone. The RDG results complement the experimental findings and demonstrate that variations in alkyl chain length significantly influence the intermolecular interactions and consequently, physicochemical properties of synthesized PILs[41].

The Frontier Molecular Orbital (FMO) analysis depicts the electronic stability and is crucial for exploring the individual parameters in energy storage and related applications. FMO analysis gives insights into the energy of the highest occupied molecular orbitals (HOMO) and lowest unoccupied molecular orbitals, and the difference between the energies of HOMO and LUMO (ΔE=LUMO-HOMO). The HOMO-LUMO energy gap gives important insights into the electronic stability and charge-transfer characteristics of the system. Molecules with a smaller HOMO-LUMO gap (ΔE=LUMO-HOMO) exhibit a high degree of polarizability[95]. The HOMO and LUMO energies, along with the HOMO-LUMO gap for the aforementioned four RTILs, are given in Figure 24. The value of ΔE is found to be 5.96 eV, 5.95 eV, 5.94 eV, and 5.95 eV for [EtPIPZ][For], [EtPIPZ][Prop], [EtPIPZ][But], and [EtPIPZ][Pent], respectively. The smaller values of ΔE indicate that the synthesised ILs have a high degree of polarizability[96,97].

The DFT results show that all the synthesized PILs possess similar electronic structure, with HOMO-LUMO energy gaps of in between 5.94-5.96 eV, indicating high electronic stability and low chemical reactivity. In contrast, the experimental density, viscosity, and ionic conductivity exhibit systematic variations with increase in alkyl chain length, as discussed in the experimental section. These variations are attributed to differences in molecular packing, free volume and intermolecular interactions rather than to changes in electronic structure of the ionic pairs. Therefore, alkyl chain elongation predominantly influences the thermophysical and transport properties of the PILs while preserving their electronic characteristics of the ionic pair[42,43].

The molecular electrostatic potential (ESP) analysis of the ETPIPZ-based ILs gives insights into the distribution of electron-deficient regions (positive potential) and electron-rich regions (negative potential). The ESP surface maps identify the electron-rich and electron-deficient regions based on a color-coded scale where the negative electrostatic potential is represented by red colour, whereas the positive potential is indicated by blue colour, and the intermediate regions are green in colour [98,99]. The calculated ESP surface ranges were found to be -5.274 e^{-2} to +5.274 e^{-2} for [EtPIPZ][For], -5.266 e^{-2} to +5.266 e^{-2} for [EtPIPZ][Prop], -5.246 e^{-2} to +5.246 e^{-2} for [EtPIPZ][But], and -5.327 e^{-2} to +5.327 e^{-2} for [EtPIPZ][Pent]. The mapped ESP surfaces of ETPIPZ-based ILs are shown in Figure 25, and it is clearly visible that the electron–rich regions (red) are localised on the oxygen atoms of the carboxylate moiety, whereas the electron-deficient regions (blue and green) are localised over the protonated nitrogen centre of the ethyl-piperazine cation. This distribution supports the presence of strong electrostatic interactions between the carboxylate anion and piperazinium cation in these ILs [100,101].

The DFT results support the experimentally observed thermophysical trends. Although the HOMO-LUMO energy gaps and ESP distributions remain nearly unchanged, indicating similar electronic properties across the synthesised PILs, the interaction energies become less negative and RDG analysis reveals progressively weaker intermolecular interactions with increasing alkyl chain length. These computational findings are consistent with the experimentally observed decrease in density, ionic

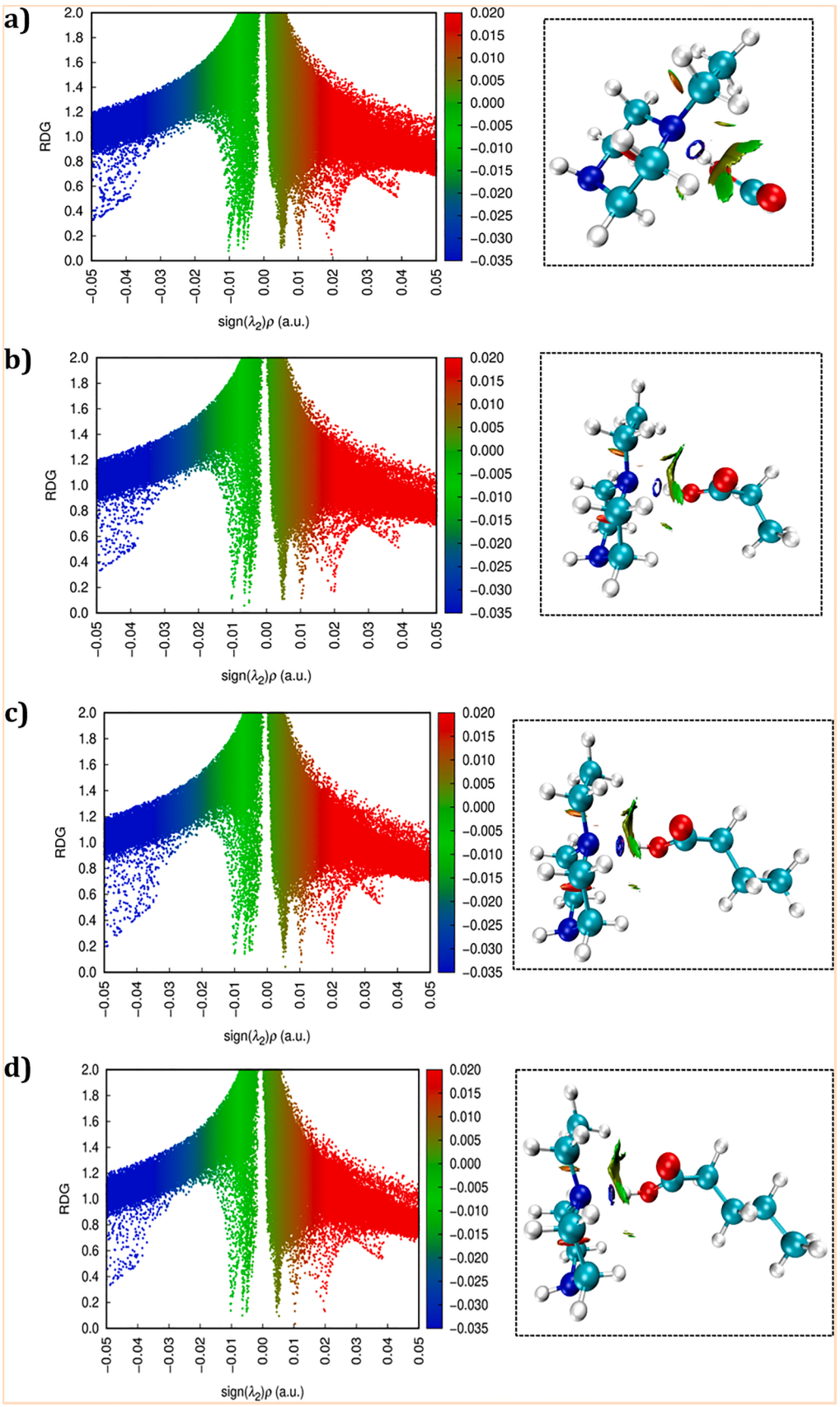

Figure 23. RDG isosurfaces and scatter plots of a) [EtPIPZ][For], b) [EtPIPZ][Prop], c) EtPIPZ] [But], and [EtPIPZ][Pent].

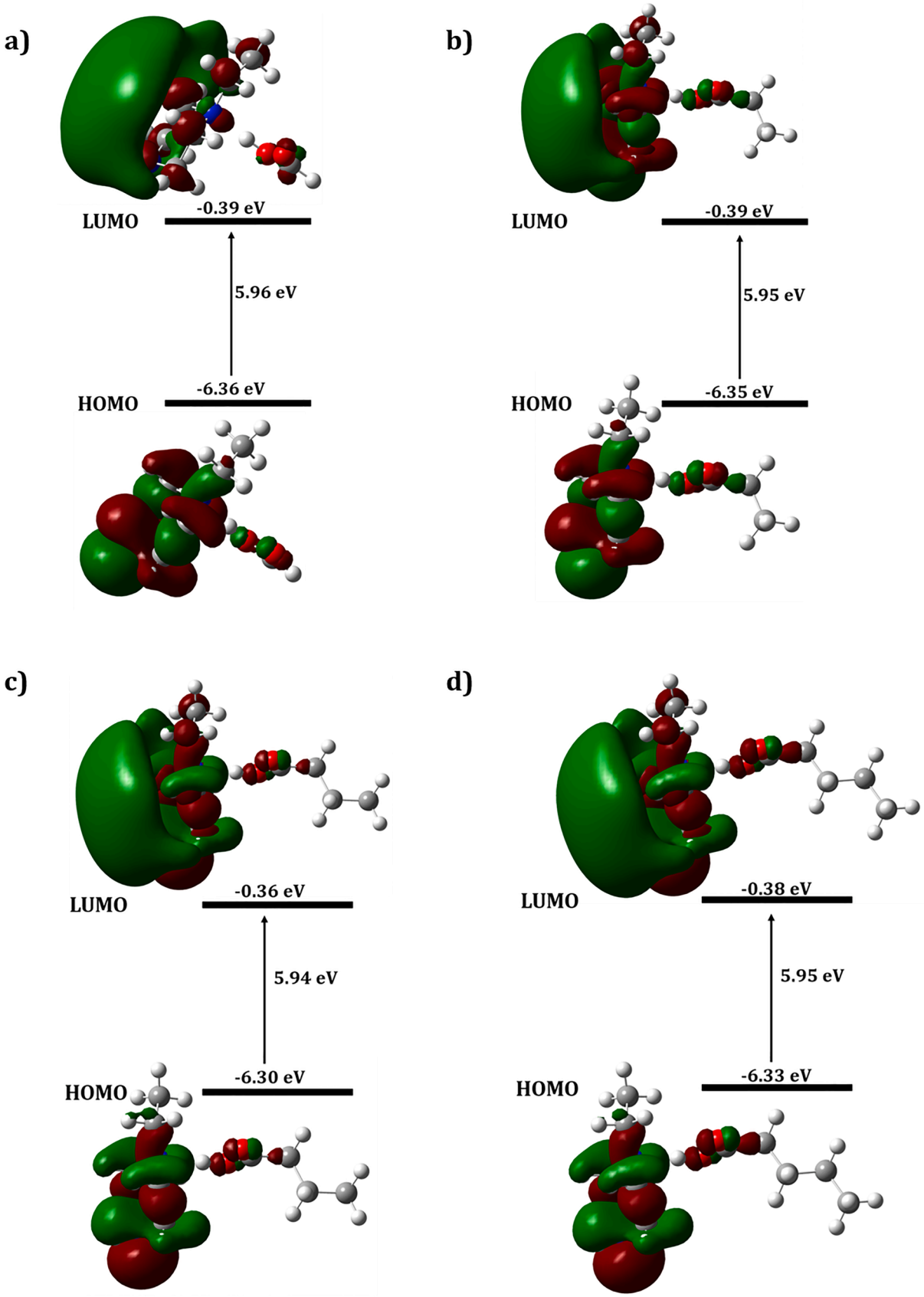

Figure 24. HOMO and LUMO for ILs a) [EtPIPZ][For], b) [EtPIPZ][Prop], c) EtPIPZ] [But], and [EtPIPZ][Pent], calculated at the 6-311 ++ G (d, p) level of theory.

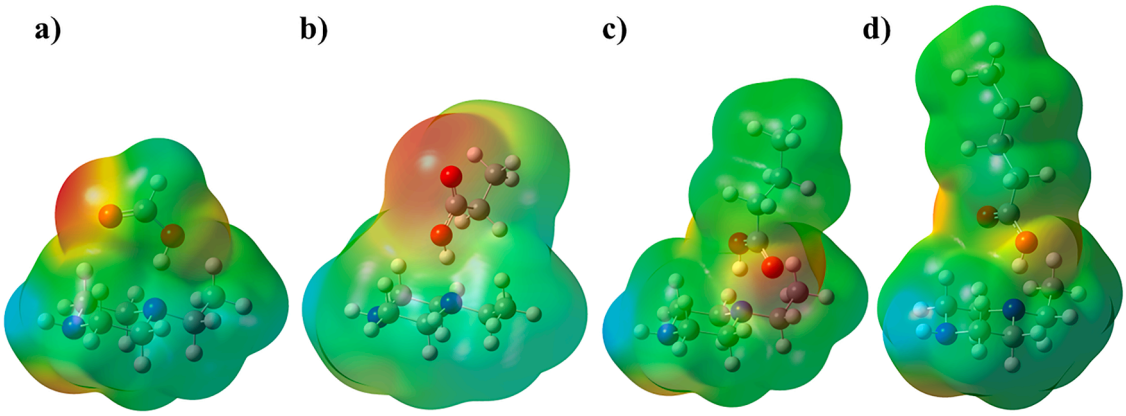

Figure 25. ESP Mapping of ILs a) [EtPIPZ][For], b) [EtPIPZ][Prop], c) EtPIPZ] [But], and [EtPIPZ][Pent], calculated at the 6-311 ++ G (d, p) level of theory.

conductivity and increase in viscosity, confirming that the physicochemical properties of the synthesised PILs are governed primarily by structural organisation and intermolecular interactions rather than by changes in their intrinsic electronic structure.

4. Conclusions

This study presents a systematic evaluation of N-ethyl piperaziniumbased PILs with carboxylate anions of varying chain length, and it reveals the influence of subtle structural modifications on the physicochemical properties. The acetate and hexanoate-based ILs were solid at room temperature whereas the formate, propanoate, butanoate and pentanoate derivatives fall under the category of room temperature ionic liquids (RTILs). The physical nature of the IL arises from an intricate balance between the intermolecular forces, ion packing efficiency, molecular symmetry, and entropy. The solid nature of [EtPIPZ][Ace] implies the presence of strong hydrogen bonding and hence efficient ionic packing. The liquid nature of [EtPIPZ][For], [EtPIPZ][Prop], [EtPIPZ][But], and [EtPIPZ][Pent] may arise from the disrupted packing and higher entropy, while the crystalline nature of [EtPIPZ][Hex] implies the dominance of van der Waals interactions due to the longer alkyl chain. Density, viscosity, speed of sound, ionic conductivity, and refractive index were measured for the four RTILs in the temperature range 293.15−323.15 K, and volumetric properties such as entropy (S), lattice potential energy (U_{POT}), free volume (V_f), and molar refraction (R_m) were computed from experimental density and refractive index data. An increase in the carboxylate anion chain length is accompanied by a decrease in the lattice potential energy and sound velocity and a corresponding increase in molecular volume, entropy, isentropic compressibility, and free volume, indicating a gradual shift from tightly associated ionic networks toward more loosely packed liquid structures. With an increase in the size of anion, the viscosity and ionic conductivity decrease, thereby indicating the competing influence of bonding and dispersion forces on ion mobility. However, results indicate that the physicochemical properties of these protic ionic liquids are influenced by both the anion structure and the intermolecular interactions within the liquid. The gradual increase in viscosity with increasing alkyl-chain length suggests that enhanced dispersion forces and greater resistance to ion movement are the primary factors governing the transport behaviour of this homologous series. The thermal behaviour of the ILs was evaluated by TGA and DSC. TGA revealed the stability of the ILs up to the temperature range 373 K - 423 K, beyond which gradual decomposition commences. Further, theoretical insights into the formation of four RTILs have been explored by DFT calculations. The ability to tune the properties of piperazine-based PILs by tuning the carboxylate anion chain length makes this class of RTILs promising candidates in domains like solvent systems, electrolyte formulations, separation processes, etc. that demand tailoring of physicochemical properties.

Supporting Information

^{1}H NMR and ^{13}C NMR, FT-IR spectra for EtPIPZ- based PILs; TGA and DTG curves of synthesized ILs, data on molar volume, sound velocity, isentropic compressibility, free volume, kinematic viscosity, and ionic conductivity parameters available in tabular format for the studied PILs.

CRediT authorship contribution statement

K. Devaiah: Writing – original draft, Validation, Methodology, Investigation, Formal analysis, Data curation, Conceptualization. **Neha Rani Kumar:** Writing – original draft, Validation, Methodology, Formal analysis, Data curation, Conceptualization. **Ramesh L. Gardas:** Writing – review & editing, Supervision, Resources, Project administration, Methodology, Funding acquisition, Conceptualization.

Declaration of competing interest

The authors declare that they have no known competing financial interests or personal relationships that could have appeared to influence the work reported in this paper.

Acknowledgements

Ramesh L. Gardas thankfully acknowledges IIT Madras for the financial support project number RF24250524CYRFER008452, and financial support from the Science and Engineering Research Board (SERB), DST, India, under project CRG/2023/003040. K. Devaiah thanks IIT Madras for the research fellowship.NRK acknowledges IAS-INSA-NASI for the Summer Research Fellowship, 2025, and members of Dhemaji College.

Supplementary materials

Supplementary material associated with this article can be found, in the online version, at doi:10.1016/j.ctta.2026.100349.

Data availability

Additionala Data Provided as Supporting Information file.

References

[1] S. Bulut, P. Klose, M.M. Huang, P.J. Dyson, G. Laurenczy, C. Friedrich, J. Menz, K. Kümmerer, I. Krossing, Synthesis of room-temperature ionic liquids with the weakly coordinating [Al(ORF)4]- Anion (RF=C(H)(CF 3)2) and the determination of their principal physical properties, Chemistry - A European Journal 16 (2010) 13139–13154, https://doi.org/10.1002/chem.201000982.
[2] M.A. Alreshidi, K.K. Yadav, S. Gunasekaran, A. Gacem, P. Sambandam, G. Subbiah, J.K. Bhutto, S. Palanivel, A.M. Fallatah, M.A. Abo El-Khair, J.

F. Almalawi, M.W. Alam, T. Perumal, S. Annadurai, A review on the evolution of ionic liquids: Sustainable synthesis, applications, and future prospects, Materials Today Sustainability 31 (2025), https://doi.org/10.1016/j.mtsust.2025.101160.
[3] R. Markiewicz, A. Klimaszyk, M. Jarek, M. Taube, P. Florczak, M. Kempka, Z. Fojud, S. Jurga, Influence of alkyl chain length on thermal properties, structure, and self-diffusion coefficients of alkyltriethylammonium-based ionic liquids, Int. J. Mol. Sci. 22 (2021), https://doi.org/10.3390/ijms22115935.
[4] A. Zamir, K.A. Elraies, M.H. Rasool, M. Ahmad, M. Ayoub, M.A. Abbas, I. Ali, Influence of alkyl chain length in ionic liquid-based drilling mud for rheology modification: a review, J. Pet. Explor. Prod. Technol. 12 (2022) 485–492, https://doi.org/10.1007/s13202-021-01343-7.
[5] A. Aljasmi, A.S. AlJimaz, K.H.A.E. AlKhaldi, A.A. Mohammad, Influence of Temperature, Anions, and Alkyl Chain Length on the Density, Viscosity, Speed of Sound, Surface Tension, and Refractive Index of Imidazolium Hexafluorophosphate-Based Ionic Liquids, J. Chem. Eng. Data 69 (2024) 1564–1577, https://doi.org/10.1021/acs.jced.4c00037.
[6] X. Zhu, Z. Chen, H. Ai, Amine-functionalized ionic liquids for CO 2 capture, (n. d.). https://doi.org/10.1007/s00894-020-04563-6/Published.
[7] M.S. Raja Shahrom, A.R. Nordin, C.D. Wilfred, The improvement of activated carbon as CO2 adsorbent with supported amine functionalized ionic liquids, J. Environ. Chem. Eng. 7 (2019), https://doi.org/10.1016/j.jece.2019.103319.
[8] J. Li, H. Wang, G. Zhou, Z.S. Wang, Hydroxyethyl and ester co-functionalized imidazolium iodide for highly efficient solid-state dye-sensitized solar cells, Chemical Communications 49 (2013) 9446–9448, https://doi.org/10.1039/c3cc44940h.
[9] M. Singh, R. Kaur, S. Kumar, V.K. Aswal, G. Singh, T.S. Kang, Self-Assembly of 2-Hydroxyethyl-1H-imidazolium-Based Surface Active Ionic Liquids and Utilization of Their Aqueous Solution in Superactivity of Cytochrome-c, Journal of Physical Chemistry B 129 (2025) 6661–6673, https://doi.org/10.1021/acs.jpcb.5c01449.
[10] M. Fathi, An Update Review on Ionic Liquids Applications in Electrochemical Sensors. http://www.JCBMS.org, 2026.
[11] H. Xing, F. Yu, X. Li, Y. Bao, W. Ye, C. Li, S. Zheng, M. Huang, Application of ionic liquids in CO2 capture and conversion: A review, Sep. Purif. Technol. 360 (2025), https://doi.org/10.1016/j.seppur.2024.130981.
[12] A.T.A. Imeer, A.A.H. Kadhum, S.D. Ahmed, H.A. Al-Bahrani, R.M. Mhaibes, G. Shu, Recent Updates on Pd-Incorporated Ionic Liquids Catalyzed Suzuki Cross-Coupling Reaction: A Mini-Review, Appl. Organomet. Chem. 39 (2025), https://doi.org/10.1002/aoc.7819.
[13] J. Pereira, R. Souza, A. Moita, A Review of Ionic Liquids and Their Composites with Nanoparticles for Electrochemical Applications, Inorganics (Basel) (2024) 12, https://doi.org/10.3390/inorganics12070186.
[14] D. Xu, X.N. Wang, L. Wang, L. Dai, C. Yang, Investigations on the Synthesis of Chiral Ionic-Liquid-Supported Ligands and Corresponding Transition-Metal Catalysts: Strategy and Experimental Schemes, Molecules 29 (2024), https://doi.org/10.3390/molecules29235661.
[15] D. Xu, X.N. Wang, L. Wang, L. Dai, C. Yang, Investigations on the Synthesis of Chiral Ionic-Liquid-Supported Ligands and Corresponding Transition-Metal Catalysts: Strategy and Experimental Schemes, Molecules 29 (2024), https://doi.org/10.3390/molecules29235661.
[16] J. Bailey, E.L. Byrne, P. Goodrich, P. Kavanagh, M. Swadźba-Kwaśny, Protic ionic liquids for sustainable uses, Green Chemistry 26 (2023) 1092–1131, https://doi.org/10.1039/d3gc03297c.
[17] S.P. Verevkin, D.H. Zaitsau, R. Ludwig, Aprotic Ionic Liquids: A Framework for Predicting Vaporization Thermodynamics, Molecules 27 (2022), https://doi.org/10.3390/molecules27072321.
[18] K. Low, S.Y.S. Tan, E.I. Izgorodina, An ab initio study of the structure and energetics of hydrogen bonding in ionic liquids, Front. Chem. 7 (2019), https://doi.org/10.3389/fchem.2019.00208.
[19] P. Stange, S.P. Verevkin, R. Ludwig, Combined Spectroscopic, Thermodynamic, and Theoretical Approach for Detecting and Quantifying Hydrogen Bonding and Dispersion Interaction in Ionic Liquids, Acc. Chem. Res. 56 (2023) 3441–3450, https://doi.org/10.1021/acs.accounts.3c00530.
[20] R. Zulfiqar, D. Ali, M.A. Ali, A. Yousuf, M. Sarfraz, A. Rauf, H.L. Xu, M. Arshad, Design and Prediction Physicochemical Properties of Piperazinium and Imidazolidinium Based Ionic Liquids: A DFT and Docking Studies, ChemistrySelect 10 (2025), https://doi.org/10.1002/slct.202405487.
[21] A. Fazal, U. Rafique, S. Laraib, A. Iqtidar, Imminent prognosis for piperazinium-based ionic liquids applications for coal desulfurization, Fuel 378 (2024), https://doi.org/10.1016/j.fuel.2024.132918.
[22] Y. Jiang, Y. Chen, F. Yang, J. Fan, J. Li, Z. Yang, X. Ji, Efficient SO2 removal using aqueous ionic liquid at low partial pressure, Chin. J. Chem. Eng. 58 (2023) 355–363, https://doi.org/10.1016/j.cjche.2022.09.021.
[23] X. Lu, B. Wang, L. Zou, New aqueous two-phase system formed by piperazinium-based surface-active ionic liquid for extraction of dyes, J. Mol. Liq. 396 (2024), https://doi.org/10.1016/j.molliq.2024.124075.
[24] X. Lu, L. Yue, M. Hu, Q. Cao, L. Xu, Y. Guo, S. Hu, W. Fang, Piperazinium-based ionic liquids with lactate anion for extractive desulfurization of fuels, Energy and Fuels (2014) 1774–1780, https://doi.org/10.1021/ef402154j.
[25] A. Gallastegui, G. Lingua, N. Lopez-Larrea, R. Carfora, D. Pasini, D. Mantione, D. Mecerreyes, Piperazinium Poly(Ionic Liquid)s as Solid Electrolytes for Lithium Batteries, Macromol. Rapid Commun. 45 (2024), https://doi.org/10.1002/marc.202400184.
[26] I. Das, K.R. Swami, R.L. Gardas, Exploring the potential of ethylenediamine based protic ionic liquids for carbon capture: A study on thermophysical properties and CO2 absorption behavior, Chemical Thermodynamics and Thermal Analysis 15 (2024), https://doi.org/10.1016/j.ctta.2024.100138.
[27] I. Das, K. Rama Swami, R.L. Gardas, Influence of alkyl substituent on thermophysical properties and CO2 absorption studies of diethylenetriamine-based ionic liquids, J. Mol. Liq. 371 (2023), https://doi.org/10.1016/j.molliq.2022.121114.
[28] S. Kalhor, A. Fattahi, Design of carboxylate-based ionic liquids (ILs) containing OH and CF3groups; influence of intramolecular hydrogen bonds and inductive effect on the binding energy between the cation and anion of ILs, a DFT study, New Journal of Chemistry 45 (2021) 4710–4723, https://doi.org/10.1039/d0nj04176a.
[29] B.R. Dash, A.K. Mishra, R.L. Gardas, Impact of Carboxylate Anion Chain Length and Temperature on Physicochemical Properties of Butyrolactam-Based Protic Ionic Liquids, J. Chem. Eng. Data 70 (2025) 2947–2960, https://doi.org/10.1021/acs.jced.4c00651.
[30] N. Scaglione, J. Avila, E. Bakis, A. Padua, M.C. Gomes, Alkylphosphonium carboxylate ionic liquids with tuned microscopic structures and properties, Physical Chemistry Chemical Physics (2023), https://doi.org/10.1039/d3cp01009k.
[31] M. Biswas, M. Dule, P.N. Samanta, S. Ghosh, T.K. Mandal, Imidazolium-based ionic liquids with different fatty acid anions: Phase behavior, electronic structure and ionic conductivity investigation, Physical Chemistry Chemical Physics 16 (2014) 16255–16263, https://doi.org/10.1039/c4cp01324g.
[32] T.D.N. Reddy, B.S. Mallik, Protic ammonium carboxylate ionic liquids: Insight into structure, dynamics and thermophysical properties by alkyl group functionalization, Physical Chemistry Chemical Physics 19 (2017) 10358–10370, https://doi.org/10.1039/c6cp08884h.
[33] B.R. Dash, A.K. Mishra, R.L. Gardas, Impact of Carboxylate Anion Chain Length and Temperature on Physicochemical Properties of Butyrolactam-Based Protic Ionic Liquids, J. Chem. Eng. Data 70 (2025) 2947–2960, https://doi.org/10.1021/acs.jced.4c00651.
[34] D. Keshapolla, N. Devunuri, S.P. Ijardar, R.L. Gardas, Influence of anion structure on volumetric properties of dilute binary systems containing carboxylate functioned trihexylammonium ionic liquids in toluene /dodecane, J. Mol. Liq. 391 (2023), https://doi.org/10.1016/j.molliq.2023.123252.
[35] M.L. Alcantara, G.L. Bressan, P.V.A. Santos, M.F.V. Nobre, J.A.P. Coutinho, C.A. O. Nascimento, L.A. Follegatti-Romero, Density and viscosity of alkylammonium ionic liquids: Experimental and COSMO-RS, J. Mol. Liq. 417 (2025), https://doi.org/10.1016/j.molliq.2024.126616.
[36] S. Jin, X. Fan, C. Stamper, R.A. Mole, Y. Yu, L. Hong, D. Yu, M. Baggioli, On the temperature dependence of the density of states of liquids at low energies, Sci. Rep. 14 (2024), https://doi.org/10.1038/s41598-024-69504-2.
[37] Y. Yu, Y. Chen, Density Prediction of Ionic Liquids at Different Temperatures Using the Average Free Volume Model, ACS Omega 6 (2021) 14869–14874, https://doi.org/10.1021/acsomega.1c00547.
[38] Y.F. Rodríguez, S. Aparicio, J.L. Trenzado, Properties and Intermolecular Forces of Ionic Liquid Mixtures: The Archetypical Case of [EMIM][BF4] + [EMIM][EtSO4], Ind. Eng. Chem. Res. 64 (2025) 1774–1791, https://doi.org/10.1021/acs.iecr.4c02839.
[39] Q. Zhang, S. Feng, X. Zhang, Y. Wei, Thermodynamic properties and intermolecular interactions of ionic liquids [DEME][BF4] or [DEME][TFSI] and their binary mixture systems with GBL, J. Mol. Liq. 328 (2021), https://doi.org/10.1016/j.molliq.2021.115373.
[40] X. Dai, X. Qiang, Estimation of the Thermophysical Properties of Pentaalkylguanidinium-Based Magnetic Ionic Liquids with Unusual Thermal Expansion Coefficient, ChemPhysChem 24 (2023), https://doi.org/10.1002/cphc.202300315.
[41] B.K. Chennuri, V. Losetty, C.D. Wilfred, R.L. Gardas, Thermophysical properties of N-phenyl-N-ethanol ammonium carboxylate based ionic liquids: Measurements, correlations and COSMO-RS study, J. Mol. Liq. 241 (2017) 246–254, https://doi.org/10.1016/j.molliq.2017.06.010.
[42] A.H. Ab Rahim, N.M. Yunus, Z. Jaffar, M.F. Allim, N.Z. Othman Zailani, S. A. Mohd Fariddudin, N. Abd Ghani, M. Umar, Synthesis and characterization of ammonium-based protic ionic liquids for carbon dioxide absorption, RSC Adv 13 (2023) 14268–14280, https://doi.org/10.1039/d3ra01345f.
[43] B.K. Chennuri, R.L. Gardas, Measurement and correlation for the thermophysical properties of hydroxyethyl ammonium based protic ionic liquids: Effect of temperature and alkyl chain length on anion, Fluid Phase Equilib 427 (2016) 282–290, https://doi.org/10.1016/j.fluid.2016.07.022.
[44] A.S. Khan, Z. Man, M.A. Bustam, G. Gonfa, F.K. Chong, Z. Ullah, A. Nasrullah, A. Sarwono, P. Ahmad, N. Muhammad, Effect of Structural Variations on the Thermophysical Properties of Protic Ionic Liquids: Insights from Experimental and Computational Studies, J. Chem. Eng. Data 62 (2017) 2993–3003, https://doi.org/10.1021/acs.jced.6b00450.
[45] Y. Shi, S. Liu, S. Wang, Y. Yu, X. Chen, X. Zhu, Thermodynamic properties of DBN-based ionic liquids and their binary mixtures with primary alcohols, J. Mol. Liq. 371 (2023), https://doi.org/10.1016/j.molliq.2022.121060.
[46] U. Preiss, V.N. Emel'yanenko, S.P. Verevkin, D. Himmel, Y.U. Paulechka, I. Krossing, Temperature-Dependent Prediction of the Liquid Entropy of Ionic Liquids, ChemPhysChem 11 (2010) 3425–3431, https://doi.org/10.1002/cphc.201000614.
[47] T. Hanke, A.L. Upterworth, D. Sebastiani, Explicit Configurational Entropy of Mixing in Molecular Dynamics Simulations, Journal of Physical Chemistry Letters 15 (2024) 11320–11327, https://doi.org/10.1021/acs.jpclett.4c02819.
[48] J. Wu, M. Hong, R. Zhang, X. Chen, J. Tong, Study on physicochemical properties of hydroxyl-functionalized ionic liquids, J. Mol. Liq. 411 (2024), https://doi.org/10.1016/j.molliq.2024.125786.

[49] B.M. Abraham, D.W. Osborne, Experimental Determination of the Molar Volume and Derivation of the Expansion Coefficient, Entropy Change on Compression, Compressibility, and First-Sound Velocity for Liquid 3He from 35 to 1200 mK and from the Saturation Pressure to 24 atm*, 1971.
[50] U.P.R.M. Preiss, J.M. Slattery, I. Krossing, In silico prediction of molecular volumes, heat capacities, and temperature-dependent densities of ionic liquids, Ind. Eng. Chem. Res. 48 (2009) 2290–2296, https://doi.org/10.1021/ie801268a.
[51] S. Panda, K. Das, V. Singh, N. Deenadayalu, R.L. Gardas, Volumetric and compressibility studies of monosaccharides in aqueous cholinium propanoate [Chl][Pro] solutions at different temperatures, J. Mol. Liq. 298 (2020), https://doi.org/10.1016/j.molliq.2019.111955.
[52] H.D.B. Jenkins, D. Tudela, L. Glasser, Lattice potential energy estimation for complex ionic salts from density measurements, Inorg. Chem. 41 (2002) 2364–2367, https://doi.org/10.1021/ic011216k.
[53] L. Glasser, Lattice and phase transition thermodynamics of ionic liquids, Thermochim. Acta 421 (2004) 87–93, https://doi.org/10.1016/j.tca.2004.03.015.
[54] A. Sarkar, G. Sharma, D. Singh, R.L. Gardas, Effect of anion on thermophysical properties of N,N-diethanolammonium based protic ionic liquids, J. Mol. Liq. 242 (2017) 249–254, https://doi.org/10.1016/j.molliq.2017.07.025.
[55] I. Das, K.R. Swami, R.L. Gardas, Exploring the potential of ethylenediamine based protic ionic liquids for carbon capture: A study on thermophysical properties and CO2 absorption behavior, Chemical Thermodynamics and Thermal Analysis 15 (2024), https://doi.org/10.1016/j.ctta.2024.100138.
[56] M. Dzida, E. Zorębski, M. Zorębski, M. Żarska, M. Geppert-Rybczyńska, M. Chorążewski, J. Jacquemin, I. Cibulka, Speed of Sound and Ultrasound Absorption in Ionic Liquids, Chem. Rev. 117 (2017) 3883–3929, https://doi.org/10.1021/acs.chemrev.5b00733.
[57] J. Pilarz, I. Polishuk, M. Chorążewski, Prediction of sound velocity for selected ionic liquids using a multilayer feed-forward neural network, J. Mol. Liq. 347 (2022), https://doi.org/10.1016/j.molliq.2021.118376.
[58] P.J. Sahandi, M. Salimi, D. Iranshahi, Insights on the speed of sound in ionic liquid binary mixtures: Investigation of influential parameters and construction of predictive models, J. Mol. Liq. 326 (2021), https://doi.org/10.1016/j.molliq.2020.115067.
[59] A. Sirohi, A. Upmanyu, P. Kumar, M. Dhiman, K.C. Juglan, D.P. Singh, K. K. Saxena, A. Bhadauria, M.I. Haque Siddiqui, Estimation of Ultrasonic Velocity, Density, Internal Pressure, and Thermophysical Parameters of Ionic Liquid Mixtures: Application of Flory's Statistical Theory, ACS Omega 9 (2024) 19363–19377, https://doi.org/10.1021/acsomega.4c00520.
[60] P.K. Chhotaray, R.L. Gardas, Thermophysical properties of ammonium and hydroxylammonium protic ionic liquids, Journal of Chemical Thermodynamics 72 (2014) 117–124, https://doi.org/10.1016/j.jct.2014.01.004.
[61] A. Basaiahgari, R.L. Gardas, Ionic liquid–based aqueous biphasic systems as sustainable extraction and separation techniques, Curr. Opin. Green Sustain. Chem. 27 (2021), https://doi.org/10.1016/j.cogsc.2020.100423.
[62] M. Kaur, S. Chauhan, Volumetric and Compressibility Studies of Ionic Surfactants in Aqueous Solutions of Tetraalkylammonium Cation-Based Ionic Liquids, J. Chem. Eng. Data 65 (2020) 3438–3447, https://doi.org/10.1021/acs.jced.9b01184.
[63] L.H.G. de Medeiros, M.A.M. de Sousa, E.E.C. da Silva, M.F.L. da Costa, F. X. Feitosa, F. Costa, A.C.M. da Silva, S. Mattedi, H.B. de Sant'Ana, Thermophysical Characterization of Protic Ionic Liquids: Density Measurements, Group Contribution Method, and PC-SAFT Modeling Application, Ind. Eng. Chem. Res. 63 (2024) 16186–16197, https://doi.org/10.1021/acs.iecr.4c02480.
[64] P. Bharmoria, K. Damarla, T.J. Trivedi, N.I. Malek, A. Kumar, A reciprocal binary mixture of protic/aprotic ionic liquids as a deep eutectic solvent: Physicochemical behaviour and application towards agarose processing, RSC Adv 5 (2015) 99245–99252, https://doi.org/10.1039/c5ra22329f.
[65] K.R. Patil, D.H. Dagade, Volumetric and compressibility studies of aqueous triethylammonium based protic ionic liquids at T = 298.15 K, J. Mol. Liq. 249 (2018) 272–280, https://doi.org/10.1016/j.molliq.2017.10.137.
[66] P. Vallet, S. Bouzón-Capelo, T. Méndez-Morales, V. Gómez-González, Y. Arosa, R. de la Fuente, E. López-Lago, J.R. Rodríguez, L.J. Gallego, J.J. Parajó, J. Salgado, M. Turmine, L. Segade, O. Cabeza, L.M. Varela, On the physical properties of mixtures of nitrate salts and protic ionic liquids, J. Mol. Liq. 350 (2022), https://doi.org/10.1016/j.molliq.2022.118483.
[67] Y.F. Rodríguez, S. Aparicio, J.L. Trenzado, Properties and Intermolecular Forces of Ionic Liquid Mixtures: The Archetypical Case of [EMIM][BF4] + [EMIM][EtSO4], Ind. Eng. Chem. Res. 64 (2025) 1774–1791, https://doi.org/10.1021/acs.iecr.4c02839.
[68] T. Zhang, W.L. Ding, Y. Zhang, K. Bi, Y. Lu, L. Ji, H. He, Investigating the property and strength of intermolecular interaction in saturated and unsaturated cyclic cations constructed ionic liquids, J. Mol. Liq. 335 (2021), https://doi.org/10.1016/j.molliq.2021.116253.
[69] M. Pezeshki, M.H. Ghatee, Properties investigation of protic morpholinium-based ionic liquids by molecular dynamics simulation and quantum chemical calculations, J. Mol. Liq. 272 (2018) 554–564, https://doi.org/10.1016/j.molliq.2018.09.053.
[70] X. Kang, Y. Zhao, J. Li, Predicting refractive index of ionic liquids based on the extreme learning machine (ELM) intelligence algorithm, J. Mol. Liq. 250 (2018) 44–49, https://doi.org/10.1016/j.molliq.2017.11.166.
[71] N.H.Z.O. Zailani, N.M. Yunus, A.H. Ab Rahim, M.A. Bustam, Experimental Investigation on Thermophysical Properties of Ammonium-Based Protic Ionic Liquids and Their Potential Ability towards CO2 Capture, Molecules 27 (2022), https://doi.org/10.3390/molecules27030851.
[72] K.A. Kurnia, M.M. Taib, M.I. Abdul Mutalib, T. Murugesan, Densities, refractive indices and excess molar volumes for binary mixtures of protic ionic liquids with methanol at T = 293.15 to 313.15 K, J. Mol. Liq. 159 (2011) 211–219, https://doi.org/10.1016/j.molliq.2011.01.005.
[73] M.S. Ali, M. Tariq, Prediction of Refractive Indices of Binary Mixtures of Ionic Liquids and Water, J. Chem. (2023) 2023, https://doi.org/10.1155/2023/9934356.
[74] G. Carissimi, M.G. Montalbán, F.G. Díaz Banos, G. Víllora, Density, Refractive Index and Volumetric Properties of Water-Ionic Liquid Binary Systems with Imidazolium-Based Cations and Tetrafluoroborate, Triflate and Octylsulfate Anions at T = 293 to 343 K and p = 0.1 MPa, J. Chem. Eng. Data 64 (2019) 979–994, https://doi.org/10.1021/acs.jced.8b00854.
[75] K.A. Kurnia, M.M. Taib, M.I. Abdul Mutalib, T. Murugesan, Densities, refractive indices and excess molar volumes for binary mixtures of protic ionic liquids with methanol at T = 293.15 to 313.15 K, J. Mol. Liq. 159 (2011) 211–219, https://doi.org/10.1016/j.molliq.2011.01.005.
[76] I. Das, K.R. Swami, R.L. Gardas, Exploring the potential of ethylenediamine based protic ionic liquids for carbon capture: A study on thermophysical properties and CO2 absorption behavior, Chemical Thermodynamics and Thermal Analysis 15 (2024), https://doi.org/10.1016/j.ctta.2024.100138.
[77] E. Bakis, K. Goloviznina, I.C.M. Vaz, D. Sloboda, D. Hazens, V. Valkovska, I. Klimenkovs, A. Padua, M.Costa Gomes, Unravelling free volume in branched-cation ionic liquids based on silicon, Chem. Sci. 13 (2022) 9062–9073, https://doi.org/10.1039/d2sc01696f.
[78] A. Pinkert, K.L. Ang, K.N. Marsh, S. Pang, Density, viscosity and electrical conductivity of protic alkanolammonium ionic liquids, Physical Chemistry Chemical Physics 13 (2011) 5136–5143, https://doi.org/10.1039/c0cp02222e.
[79] H. Moslehi, S.M. Hosseini, M. Pierantozzi, M.M. Alavianmehr, B. Haghighi, Modeling the viscosity of ionic liquids using combined friction theory with perturbed hard-chain equation of state and neural network approaches, J. Mol. Liq. 383 (2023), https://doi.org/10.1016/j.molliq.2023.122004.
[80] J.L. Lebga-Nebane, S.E. Rock, J. Franclemont, D. Roy, S. Krishnan, Thermophysical properties and proton transport mechanisms of trialkylammonium and 1-alkyl-1H-imidazol-3-ium protic ionic liquids, Ind. Eng. Chem. Res. 51 (2012) 14084–14098, https://doi.org/10.1021/ie301687c.
[81] R.L. Gardas, J.A.P. Coutinho, A group contribution method for viscosity estimation of ionic liquids, Fluid Phase Equilib 266 (2008) 195–201, https://doi.org/10.1016/j.fluid.2008.01.021.
[82] E. Boli, T. Katsavrias, E. Voutsas, Viscosities of pure protic ionic liquids and their binary and ternary mixtures with water and ethanol, Fluid Phase Equilib 520 (2020), https://doi.org/10.1016/j.fluid.2020.112663.
[83] A. Kilic, A. Uzun, R. Yildirim, D. Eroglu, Ionic liquid electrolytes for metal-air batteries: High-throughput screening and machine learning modeling, Electrochim. Acta 524 (2025), https://doi.org/10.1016/j.electacta.2025.145997.
[84] M. Saha, A. Kumar, R. Kanaoujiya, K. Behera, S. Trivedi, A Comprehensive Review of Novel Emerging Electrolytes for Supercapacitors: Aqueous and Organic Electrolytes Versus Ionic Liquid-Based Electrolytes, Energy and Fuels 38 (2024) 8528–8552, https://doi.org/10.1021/acs.energyfuels.4c00685.
[85] H.N. Kwon, S.J. Jang, Y.C. Kang, K.C. Roh, The effect of ILs as co-salts in electrolytes for high voltage supercapacitors, Sci. Rep. 9 (2019), https://doi.org/10.1038/s41598-018-37322-y.
[86] R.C.Thakur Shivani, A. Thakur, A. Sharma, R. Sharma, Unravelling the prospects of electrolytes containing ionic liquids and deep eutectic solvents for next generation lithium batteries, Journal of Energy Chemistry 105 (2025) 482–500, https://doi.org/10.1016/j.jechem.2025.01.060.
[87] P. Vallet, J.J. Parajó, A. Santiago-Alonso, M. Villanueva, L.M.Varela Cabeza, J. Salgado, Anomalous behaviour of the ionic conductivity of nanoconfined IL -lithium salt mixtures, J. Mol. Liq. 401 (2024), https://doi.org/10.1016/j.molliq.2024.124630.
[88] W. Xiong, Z. Yin, X. Zhang, Z. Tu, X. Hu, Y. Wu, Ionic Liquids Endowed with Novel Hybrid Anions for Supercapacitors, ACS Omega 7 (2022) 26368–26374, https://doi.org/10.1021/acsomega.2c02211.
[89] A.K. Verma, A.S. Thorat, J.K. Shah, Predicting Ionic Conductivity of Imidazolium-Based Ionic Liquid Mixtures Using Quantum-Mechanically Derived Partial Charges in the Condensed Phase, Journal of Physical Chemistry B 129 (2025) 2546–2559, https://doi.org/10.1021/acs.jpcb.4c08275.
[90] S. Rogalsky, O. Tarasyuk, A. Vashchuk, O. Dzhuzha, T. Cherniavska, S. Makhno, Thermophysical properties and ionic conductivity of new imidazolium-based protic ionic liquids, J. Mol. Liq. 382 (2023), https://doi.org/10.1016/j.molliq.2023.121942.
[91] T.T. Le, F. Abbas, S. Bourdo, F. Watanabe, N. Siraj, Counterion Effects of Protic Ionic Liquids on the Conductivity and Stretchability of Free-Standing PEDOT:PSS Films, Macromolecules 58 (2025) 11718–11730, https://doi.org/10.1021/acs.macromol.5c01646.
[92] E. Sedghamiz, F. Khashei, M. Moosavi, Linear tricationic ionic liquids: Insights into the structural features using DFT and molecular dynamics simulation, J. Mol. Liq. 271 (2018) 96–104, https://doi.org/10.1016/j.molliq.2018.08.111.
[93] Z.L. Seeger, E.I. Izgorodina, A Systematic Study of DFT Performance for Geometry Optimizations of Ionic Liquid Clusters, J. Chem. Theory Comput. 16 (2020) 6735–6753, https://doi.org/10.1021/acs.jctc.0c00549.
[94] H. Li, P. Zhou, J. Zhang, D. Li, X. Li, X. Gao, A theoretical guide for screening ionic liquid extractants applied in the separation of a binary alcohol-ester azeotrope through a DFT method, J. Mol. Liq. 251 (2018) 51–60, https://doi.org/10.1016/j.molliq.2017.12.049.
[95] B. Chenthamara, R.L. Gardas, Unravelling the influence of water: Investigating the physicochemical properties of deep eutectic solvents based on choline

chloride and pyruvic acid/α-keto glutaric acid, J. Mol. Liq. 416 (2024), https://doi.org/10.1016/j.molliq.2024.126489.
[96] M.A.F. Afzal, J. Hachmann, Benchmarking DFT approaches for the calculation of polarizability inputs for refractive index predictions in organic polymers, Physical Chemistry Chemical Physics 21 (2019) 4452–4460, https://doi.org/10.1039/c8cp05492d.
[97] P. Díaz-Rodríguez, J.C. Cancilla, N.V. Plechkova, G. Matute, K.R. Seddon, J. S. Torrecilla, Estimation of the refractive indices of imidazolium-based ionic liquids using their polarisability values, Physical Chemistry Chemical Physics 16 (2014) 128–134, https://doi.org/10.1039/c3cp53685h.
[98] J. Liu, S. Zhang, Y. Yao, Y. Zeng, N. Zhou, D. Luo, J. Tang, C. Wang, K. Zhang, Y. Li, J. Hu, B. Yang, C. Peng, H. Liu, Electrostatic potential characteristics of ionic liquids: A strategy for computational screening of electrolytes for Lithium metal batteries, Comput. Theor. Chem. (2025) 1252, https://doi.org/10.1016/j.comptc.2025.115379.
[99] G. Tian, K. Yuan, Performance and mechanism of alkylimidazolium ionic liquids as corrosion inhibitors for copper in sulfuric acid solution, Molecules 26 (2021), https://doi.org/10.3390/molecules26164910.
[100] F. Parveen, T. Patra, S. Upadhyayula, A structure-activity relationship study using DFT analysis of Bronsted-Lewis acidic ionic liquids and synergistic effect of dual acidity in one-pot conversion of glucose to value-added chemicals, New Journal of Chemistry 42 (2018) 1423–1430, https://doi.org/10.1039/c7nj02364b.
[101] B. Wang, M. Zhu, M. Liu, Y. Wang, Y. Zhou, J. Ma, Design of novel dual functional ionic liquids and DFT study on their CO2 absorption mechanism, J. Mol. Liq. 366 (2022), https://doi.org/10.1016/j.molliq.2022.120340.